AD-A123 125 INFLUENCE OF BLADE TIP CLEARANCE ON AERODYNAMICALLY 1/1
INDUCED VIBRATION..(U) GENERAL MOTORS CORP INDIANAPOLIS
IN DETROIT DIESEL ALLISON DI.. J L BETTNER OCT 82
UNCLASSIFIED DDA-EDR-11257 AFOSR-TR-82-1086 F/G 21/5 NL

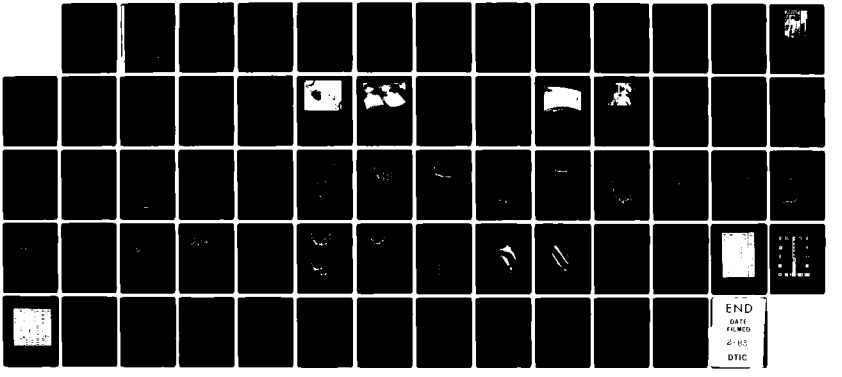

END
DATE FILMED
2-83
DTIC

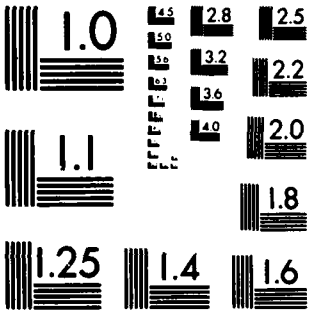

MICROCOPY RESOLUTION TEST CHART
NATIONAL BUREAU OF STANDARDS-1963-A

AFOSR-TR- 82-1086

(12)

Influence of Blade Tip Clearance on Aerodynamically Induced Vibration

James L. Bettner

Detroit Diesel Allison
Division of General Motors Corporation
P.O. Box 894
Indianapolis, IN 46206

October 1982

Final Report for Period 31 August 1981 through 30 September 1982

AD A123125

Approved for public release; distribution unlimited

Prepared for
AIR FORCE OFFICE OF SCIENTIFIC RESEARCH (AFSC)
Bolling Air Force Base
Washington, D.C.

Unclassified

SECURITY CLASSIFICATION OF THIS PAGE (When Data Entered)

REPORT DOCUMENTATION PAGE		READ INSTRUCTIONS BEFORE COMPLETING FORM
1. REPORT NUMBER AFOSR-TR- 82-1086	2. GOVT ACCESSION NO. A123125	3. RECIPIENT'S CATALOG NUMBER
4. TITLE (and Subtitle) Influence of Blade Tip Clearance on Aerodynamically Induced Vibration		5. TYPE OF REPORT & PERIOD COVERED Final Report for 31 Aug. 1981-30 Sept. 1982 6. PERFORMING ORG. REPORT NUMBER EDR 11257
7. AUTHOR(s) James L. Bettner		8. CONTRACT OR GRANT NUMBER(s) F49620-80-C-0078
9. PERFORMING ORGANIZATION NAME AND ADDRESS Detroit Diesel Allison Division of General Motors Corporation P.O. Box 894, Indianapolis, IN 46206		10. PROGRAM ELEMENT, PROJECT, TASK AREA & WORK UNIT NUMBERS 61102F 2307/A1
11. CONTROLLING OFFICE NAME AND ADDRESS Air Force Office of Scientific Research Bolling AFB, Washington, DC 20332		12. REPORT DATE October 1982 13. NUMBER OF PAGES 64
14. MONITORING AGENCY NAME & ADDRESS (if different from Controlling Office)		15. SECURITY CLASS. (of this report) Unclassified 15a. DECLASSIFICATION DOWNGRADING SCHEDULE

16. DISTRIBUTION STATEMENT (of this Report)

Approved for public release; distribution unlimited

17. DISTRIBUTION STATEMENT (of the abstract entered in Block 20, if different from Report)

18. SUPPLEMENTARY NOTES

19. KEY WORDS (Continue on reverse side if necessary and identify by block number)

Forced vibration
Aerodynamically induced vibration
Turbomachinery
Unsteady flow
Axial flow compressor
Tip clearance effects

20. ABSTRACT (Continue on reverse side if necessary and identify by block number)

An experimental investigation, whose objective was to demonstrate the influence of rotor blade tip clearance effects on the dynamic pressure induced on a downstream vane, was conducted in a large, low speed, single-stage research compressor. The blade tip clearance was 0.48% span. The rig was heavily instrumented with dynamic pressure gages on the vane hub, mean, and tip section suction and pressure surfaces. Two gages were mounted on the

(over)

DD FORM 1 JAN 73 1473 EDITION OF 1 NOV 65 IS OBSOLETE

Unclassified

SECURITY CLASSIFICATION OF THIS PAGE (When Data Entered)

20. ABSTRACT (cont)

rotor tip trailing edge suction and pressure surfaces. Radial/circumferential hot-wire surveys established the steady and dynamic flow conditions into and out of the vane.

Experimental results were compared with previously obtained results in the same facility where the blade tip clearance was 3.0%. Those evaluations showed that the reduction of blade tip clearance from 3.0% to 0.48% had a significant effect on reducing the magnitude and phase lag of the induced dynamic pressure fluctuations in the vane tip region. The results also indicated that the disturbances, generated by the large blade tip clearances, penetrated a substantial distance radially inward almost to the vane mean section.

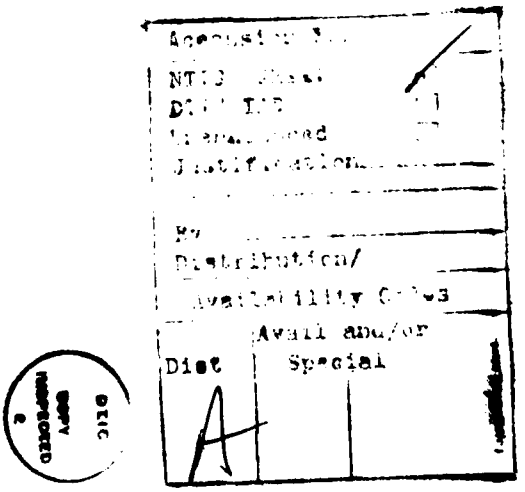

TABLE OF CONTENTS

Section	Title	Page
I	Introduction	7
II	Test Configuration and Instrumentation	8
	Test Rig Design	8
	Instrumentation	12
III	Experimental Program	22
	Steady-State Performance.	22
	Blade Tip Section Trailing Edge Dynamic Pressure Results. .	23
	Vane Inlet Conditions	25
	Vane Surface Dynamic Pressure Results	31
	Dynamic Signal Oscilloscope Traces and Harmonic Content . .	45
IV	Conclusions.	59
V	Recommendations.	61
	References	62
	List of Symbols.	63

LIST OF ILLUSTRATIONS

Figure	Title	Page
1	Low speed compressor rig facility.	10
2	Low speed compressor flow path	11
3	Low speed compressor stage steady and dynamic instrumentation	13
4	Vane mean section dynamic instrument location.	16
5	Radial and chordwise suction and pressure surface transducer instrument locations.	17
6	Location of Kulites on stator airfoils	19
7	View of typical hot-wire installation in low speed compressor vane row.	20
8	Meridian Laboratory 12-channel slip ring installed on the low speed compressor rotor face	21
9	Effect of blade tip clearance on overall stage pressure ratio/flow rate characteristics	23
10	Rotor tip section trailing edge dynamic pressure and phase lag variation with stage operating conditions, 100% speed, 0.48% span blade tip clearance.	24
11	Vane leading edge absolute velocity contours at near-design operating conditions, 0.48% span blade tip clearance. . . .	26
12	Vane leading edge air angle contours at near-design operating conditions, 0.48% span blade tip clearance.	26
13	Vane leading edge streamwise fluctuating velocity component ΔU at near-design operating conditions, 0.48% span blade tip clearance	27
14	Vane leading edge transverse fluctuating velocity component ΔV at near-design operating conditions, 0.48% span blade tip clearance	27
15	Vane leading edge streamwise fluctuating velocity component phase lag angle at near-design operating conditions, 0.48% span blade tip clearance.	28
16	Vane leading edge transverse fluctuating velocity component phase lag angle at near-design operating conditions, 0.48% span blade tip clearance.	28

LIST OF ILLUSTRATIONS (cont)

Figure	Title	Page
17	Influence of blade tip clearance on normalized transverse fluctuating velocity component at vane inlet midpassage, 100% speed.	30
18	Influence of blade tip clearance on phase angle of the normalized transverse fluctuating velocity component at vane inlet midpassage, 100% speed	31
19	Influence of blade tip clearance on dynamic pressure differential across vane near-tip section, 100% speed . . .	32
20	Influence of blade tip clearance on dynamic pressure magnitude on vane near-tip section pressure surface, 100% speed . . .	33
21	Influence of blade tip clearance on dynamic pressure magnitude on vane near-tip suction surface, 100% speed.	34
22	Influence of blade tip clearance on dynamic pressure differential across vane mean section, 100% speed	35
23	Influence of blade tip clearance on dynamic pressure differential across vane near-hub section, 100% speed	36
24	Influence of blade tip clearance on vane near-hub pressure surface dynamic pressure magnitude, 100% speed.	36
25	Influence of blade tip clearance on vane near-hub suction surface dynamic pressure magnitude, 100% speed.	37
26	Influence of blade tip clearance on dynamic pressure differential across vane leading edge, 100% speed	38
27	Influence of blade tip clearance on dynamic pressure magnitude on vane leading edge pressure surface, 100% speed. . .	38
28	Influence of blade tip clearance on dynamic pressure magnitude on vane leading edge suction surface, 100% speed . . .	39
29	Influence of blade tip clearance on dynamic pressure differential at vane trailing edge, 100% speed.	40
30	Influence of blade tip clearance on dynamic pressure differential phase lag angle at vane near-tip section, 100% speed .	41
31	Influence of blade tip clearance on dynamic pressure differential phase lag angle at vane mean section, 100% speed . . .	42
32	Influence of blade tip clearance on dynamic pressure differential phase lag angle at vane near-hub section, 100% speed .	43

LIST OF ILLUSTRATIONS (cont)

Figure	Title	Page
33	Influence of blade tip clearance on dynamic pressure differential phase lag angle at vane leading edge, 100% speed . . .	44
34	Influence of blade tip clearance on suction surface dynamic pressure phase lag angle at vane leading edge, 100% speed .	44
35	Influence of blade tip clearance on pressure surface dynamic pressure phase lag angle at vane leading edge, 100% speed .	45
36	Influence of blade tip clearance on dynamic pressure differential phase lag angle at vane trailing edge, 100% speed. . .	46
37	Unwrapped vane dynamic pressure distribution: 0.48% blade tip clearance, near-design operating conditions	47
38	Unwrapped vane phase lag distribution: 0.48% blade tip clearance, near-design operating conditions.	48
39	Vane Kulite gage and hot-wire anemometer probe locations . . .	49
40	Design flow conditions--vane leading edge hot-wire radial and circumferential survey (0.48% span tip clearance) . . .	51
41	Design flow conditions--vane suction and pressure surface Kulite gage response (0.48% span tip clearance)	52
42	Design flow conditions--vane trailing edge hot-wire radial and circumferential survey (0.48% span tip clearance) . . .	53
43	Vane surface distribution of dynamic pressure harmonic content for 0.48% blade tip clearance, near-design operating conditions, 100% speed.	55
44	Vane trailing edge plane near-tip region fluctuating velocity harmonic content for 0.48% blade tip clearance, near-design operating conditions.	57

LIST OF TABLES

Table	Title	Page
1	Low speed compressor design point.	8
2	Airfoil mean-section mechanical and aerodynamic characteristics	12
3	Axial chord location of Kulite transducers on stators.	18

I. INTRODUCTION

DDA has conducted a long range series of aerodynamically induced vibration experiments in a large, low speed, single-stage compressor. The effect of aerodynamic and geometric variables--such as interblade phase angle, reduced frequency, blade/vane axial gap, solidity, camber, and incidence--on the dynamic pressure field of a downstream vane has been investigated. The objective of these experiments has been to provide experimental data for (1) phenomenological understanding of aerodynamic induced vibration and (2) evaluation of analytical methods.

Recently, an experiment was conducted with a large blade tip clearance of 3.0% span, which showed the dynamic pressure field to be very strongly three-dimensional in the vane passage. Fluctuating velocity components on the order of 20%-30% of the freestream absolute velocity were measured in the vane leading edge hub and tip regions. In the hub region, this wake disturbance was attributed to the buildup and subsequent shedding of rotor hub endwall boundary layer flow. In the tip region, the wake pattern was thought to be controlled by the tangential flow through the large (3.0% span) blade tip clearance. The objective of the present experiment was to establish that it was, indeed, the blade tip clearance flow that was the principal forcing function of the vane tip region dynamic pressure field. For the present experiment the rotor blade tip clearance was reduced to 0.48% span and the experimental results were compared with the 3.0% span tip clearance findings. The results of those blade tip clearance investigations are presented in this report.

II. TEST CONFIGURATION AND INSTRUMENTATION

TEST RIG DESIGN

The test equipment employed in this investigation was the DDA Low Speed Compressor Facility (LSCF). The stage configuration was identical to that used in Ref. 1 except that the rotor was reworked to provide for a very small tip clearance between the blade tip end and casing wall. Blade tip section rework was accomplished by (1) bonding 0.150 in. fiberglass material to the blade tips, (2) grinding the rotor tip to give the proper end clearance, and (3) blending the attached material to exhibit the proper surface contour. An average tip clearance of 0.023 in. (0.48% blade span) was established.

The blading and flow path of the LSCF have been designed to reflect realistic aerodynamic values of blockage, blade loading and loss levels, and tip clearance, along with realistic geometric design parameters that are typical of aft stages of modern multistage compressors. Also, the Reynolds number at the compressor inlet is typical of modern compressors, i.e., greater than 200,000. The blading and flow path are physically large enough to allow high-quality, detailed endwall boundary layer measurements to be made over the entire endwall.

Resulting geometric and design point aerodynamic conditions for the low speed compressor, along with representative airfoil geometry, are listed in Table 1.

Table 1.
Low speed compressor design point.

Flow rate, $W\sqrt{\theta}/\delta$	31.01 lb/sec
Tip speed, $U_t/\sqrt{\theta}$	183.5 ft/sec
Rotational speed, $N/\sqrt{\theta}$	876.3 rpm
Stage pressure ratio, R_c	1.0125
Stage efficiency, η_{TT}	88.1%
Inlet tip diameter, D_t	48.0 in.
Hub/tip radius ratio, r_h/r_t	0.80
Blade span, ℓ	4.80 in.
Blade chord, C_b	4.589 in.
Blade aspect ratio	1.046
Blade solidity, C_b/s	1.435
Vane chord, C_v	5.089 in.
Vane aspect ratio, ℓ/C_v	0.943
Vane solidity, C_v/s	1.516

Rotor Blade Design

The rotor and stator airfoils were designed with the DDA Axial Compressor Streamline Curvature Design System. End clearance effects were computed by the method described in Ref. 2. Forty-two blades were used in the rotor design. The design features high camber with fairly large deviation angles near the hub region. Maximum thickness varies from nearly 7% of chord at the hub to 4% at the tip. The blade chord varies linearly with radius and yields a solidity of about 1.6 at the hub to 1.3 at the tip. Blade incidence was set between +1.2 to -1.0 deg limits. Fiberglass material was used for the blade profile and platform. The fiberglass material was molded around a flat steel spar that passed from the tip section of the blade down through the blade and was welded to a steel base plate. The blades are held in the wheel by a T-shaped base arrangement that allows blades to be easily changed in the wheel without disturbing the basic wheel design.

Nearly the entire axial length of the flow path features a transparent Plexiglas casing sector that covers a circumferential extent of 108 deg. This transparent casing permits a utilization of flow visualization techniques.

The assembled test rig with 1.0 aspect ratio blading is shown installed in the test facility in Figure 1. Fore and aft center bodies are supported and, hence, blade and vane end clearances are established by five struts located in the far front of the flow path and five struts located downstream of the stator. The struts for the present investigation are 10% thick 65 series symmetric airfoil contours. End clearances are 0.48% for the rotor and 0% for the tip cantilevered vanes.

Table 1 shows that both the overall rig and the airfoils are large. The large airfoils permit the detailed, accurate endwall boundary layer studies to be accomplished without having to resort to extreme miniaturization of instrumentation.

Figure 1. Low speed compressor rig facility.

Figure 2 illustrates the low speed compressor flow path, showing the blade and vane locations along with the transparent windows and the arrangement of the rotating components. The flow-path hub/tip radius ratio was held constant at 0.8 for a large distance both upstream of the rotor and downstream of the stator. This flow-path contour not only simplified inlet and exit station instrumentation design but also provided the axial length upstream of the rotor to dictate the characteristics of the rotor inlet boundary layer.

Vane Design

The vane features a large camber angle variation in the hub region, a radially constant maximum thickness/chord distribution, and incidence that varies from about 0 to -1 deg. Vane solidity varies from 1.68 at the hub to 1.35 at the tip. Forty vanes were incorporated in the stage design. Fiberglass material forms the airfoil profile. It is molded around a steel spar that passes radially through the vane and is welded to the steel trunnion. The vane/casing

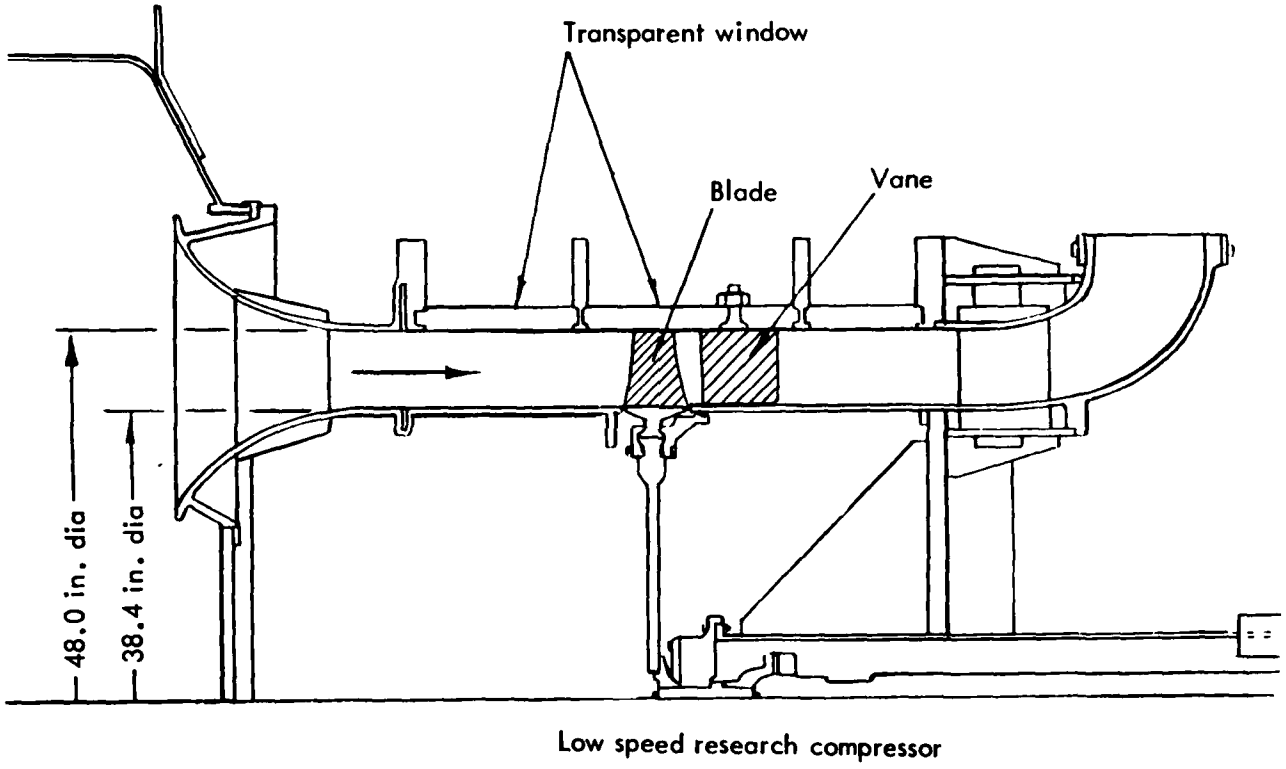

Figure 2. Low speed compressor flow path.

interface design allows the vanes to be reset over ±20 deg from design setting angle. Figure 2 shows the vanes cantilevered from the casing with a stationary endwall under the vane hub. Table 2 summarizes the compressor design by presenting mean-section aerodynamic and geometric design values.

Table 2.
Airfoil mean-section mechanical and aerodynamic characteristics.

Type of airfoil	65 series	65 series
Chord, C--in.	4.489	5.089
Solidity, σ = C/s	1.435	1.516
Camber, ϕ --deg	20.42	48.57
Aspect ratio, AR = ℓ /C	1.046	0.943
Leading edge radius/C	0.0044	0.0049
Trailing edge radius/C	0.0028	0.0030
Inlet angle, β_1--deg	59.38	37.84
Exit angle, β_2--deg	42.41	0.00
Loss coefficient, $\bar{\omega}$	0.043	0.056
Diffusion factor, D_f	0.449	0.410

INSTRUMENTATION

Steady-State Instrumentation

Steady-state instrumentation consists of multiple-element total pressure rakes distributed circumferentially around the annulus at the stage inlet, stator inlet, and stage exit planes; boundary layer rakes on the hub and tip walls at the rotor inlet and stator exit; multiple-element total temperature rakes at the stator inlet and exit; and static pressure taps distributed around the annulus on the hub and tip walls and axially through the stage. This instrumentation arrangement is illustrated in Figure 3. In addition, 15 static pressure taps are arranged on the tip wall of one stator passage to allow mapping of the vane tip static pressure distribution. The stage inlet total temperature is measured in the plenum chamber located upstream of the flow-path annulus. All of the pressure instrumentation is connected to a six-unit 48-channel Scanivalve, interfaced with a Digitec scanner and driven by a Hewlett-Packard (HP) Model 2117F computer. Differential (0-1.0 psid) Druck pressure transducers are employed in the Scanivalve. A deadweight system provides reference pressures of 0.0, 0.5, and 1.0 psia to the Scanivalve transducers for continuous on-line calibration of the pressure measurement system.

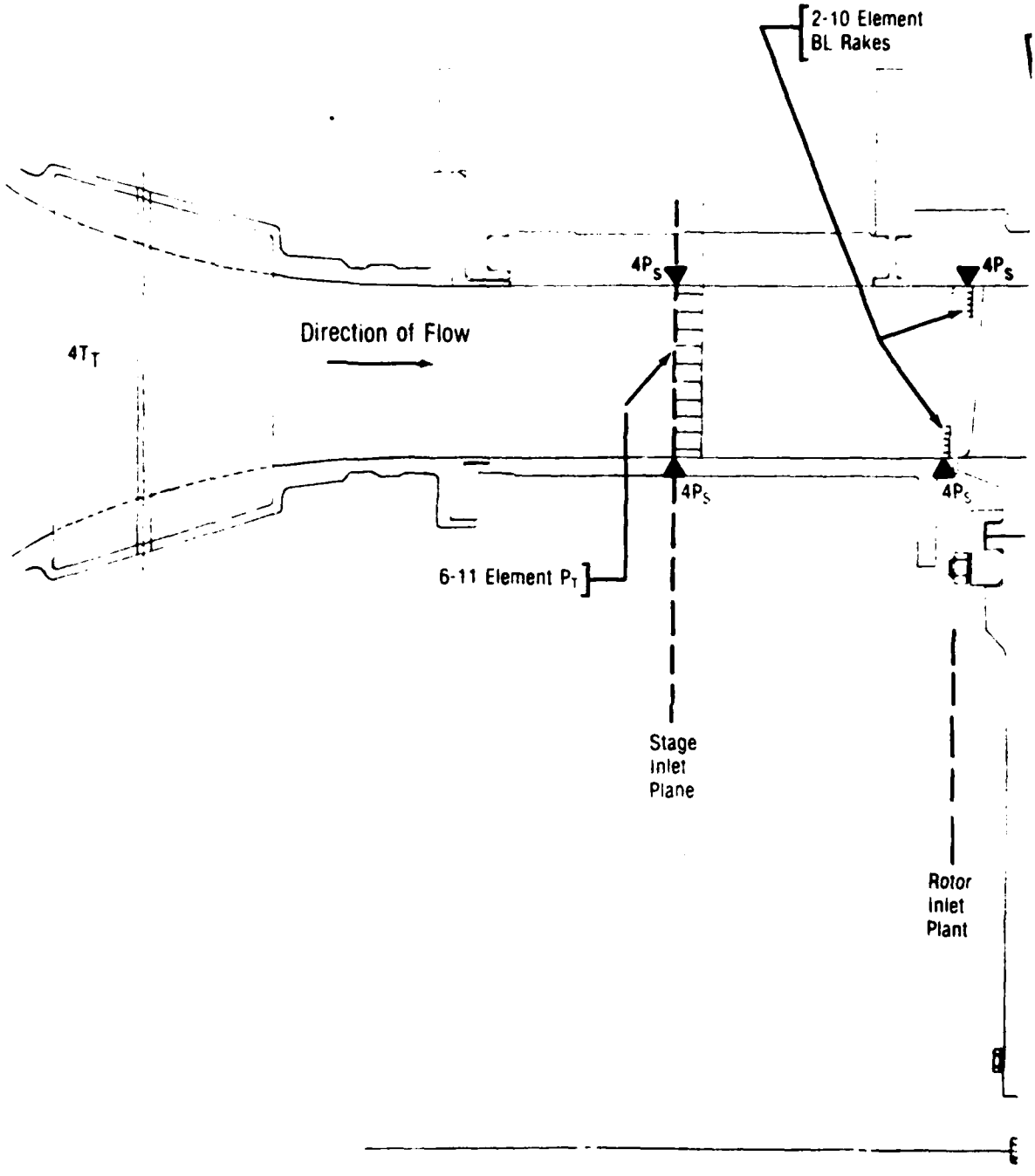
2-10 Element
BL Rakes
4Ps
4Ps
Direction of Flow
4TT
4Ps
4Ps
6-11 Element PT
Stage
Inlet
Plane
Rotor
Inlet
Plant

Fig

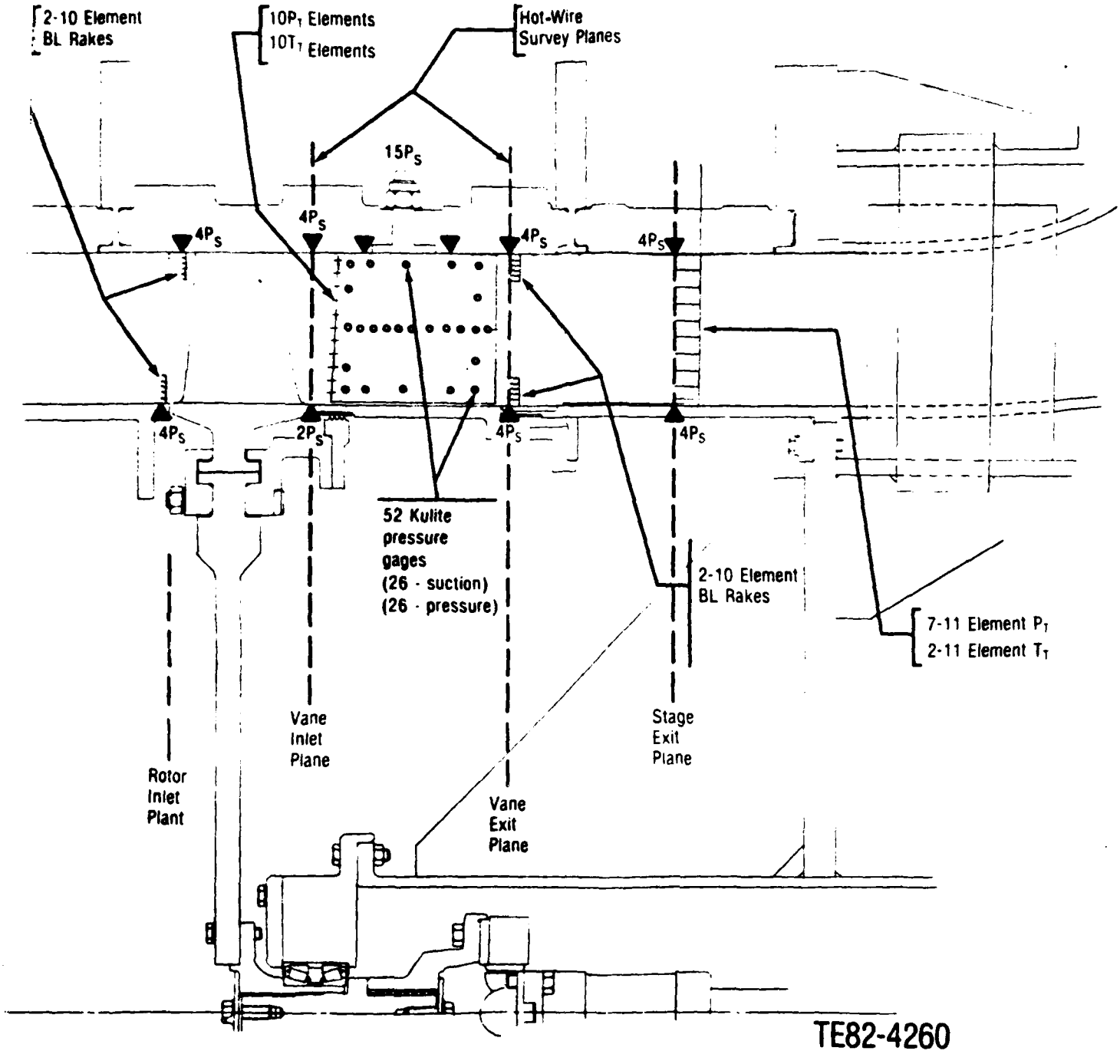

Figure 3. Low speed compressor stage steady and dynamic instrumentation.

(2)

Radial/circumferential hot-wire anemometer surveys are performed in the exit planes of the rotor and stator. In addition, radial/circumferential surveys can be performed at two axial locations inside the stator passage. Streamwise velocity and air angle are determined by positioning the probe at a fixed axial, circumferential, and radial location, and then by yawing the probe until the output voltages of the two hot wires are the same value. DISA constant-temperature hot-wire anemometry equipment is used. The outputs are linearized and compensated for temperature differences that exist between the velocity calibration jet air stream and the rig flow field environment.

Dynamic Instrumentation

For time-variant measurements, miniature pressure transducers and a crossed-wire probe are used. Kulite thin-line transducers are located on the surfaces of four stator airfoils. These transducers are flush-mounted by grooving the surface. The grooves, designed to accommodate the transducer, bonding agent, and lead wires, extend from the particular transducer through the stator trunnion. The grooves are clearly seen in Figure 4 on two of the mean-section instrumented airfoils used in this experimental program. Figure 5 shows the location of the Kulite pressure transducers on the hub and tip sections and leading and trailing edge regions of two additional instrumented airfoils. Table 3 lists radial and axial locations of the gages on the stator airfoils. Figure 6 is a schematic of the instrumented airfoils and shows the numbering system used. A view of the crossed-wire probe used in the experiment is shown in Figure 7. In this photograph the wire is located near the center span instrumented airfoils.

In addition to the dynamic instrumentation installed on the vane suction and pressure surfaces, two LQL-080-505 Kulite gages were installed on the rotor suction and pressure surfaces, respectively, at the blade trailing edge tip section. Signals from these gages were led out through a Meridian Laboratory Model SN-12 12-channel mercury bath slip ring assembly, which is shown installed on the LSCF rotor face in Figure 8.

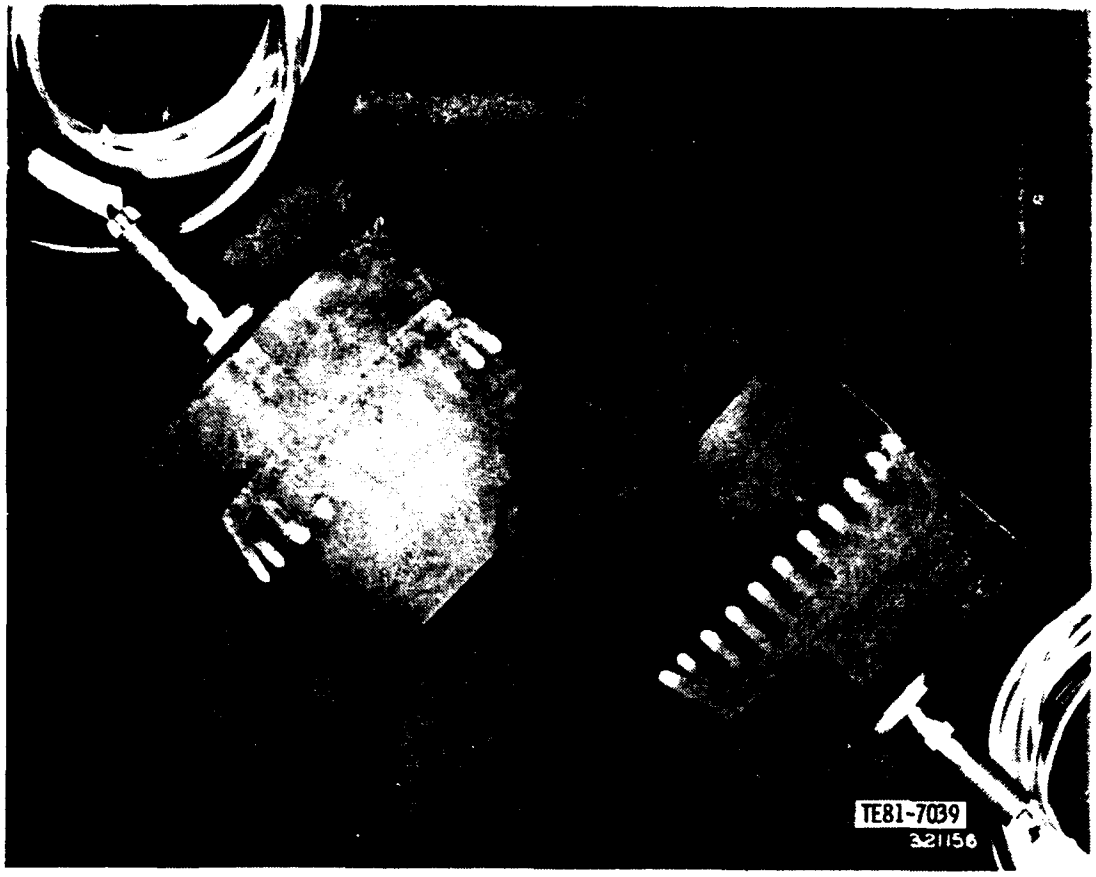

Figure 4. Vane mean section dynamic instrument locations.

Data Acquisition System

The central element in the acquisition of the time-variant and steady-state data in this experiment is a digital computer with its specialized peripheral hardware. An HP Model 2117F computer operating under RTE1VB software is used with a Preston GMAD-2 analog-to-digital (A/D) conversion system to acquire data at a rate of 50,000 points per sec for each of the transducers. For data acquisition in the steady-state mode, the computer is interfaced with a Digitec scanner, which allows conversion of Scanivalve voltages to appropriate pressures as well as calculation of operating temperatures.

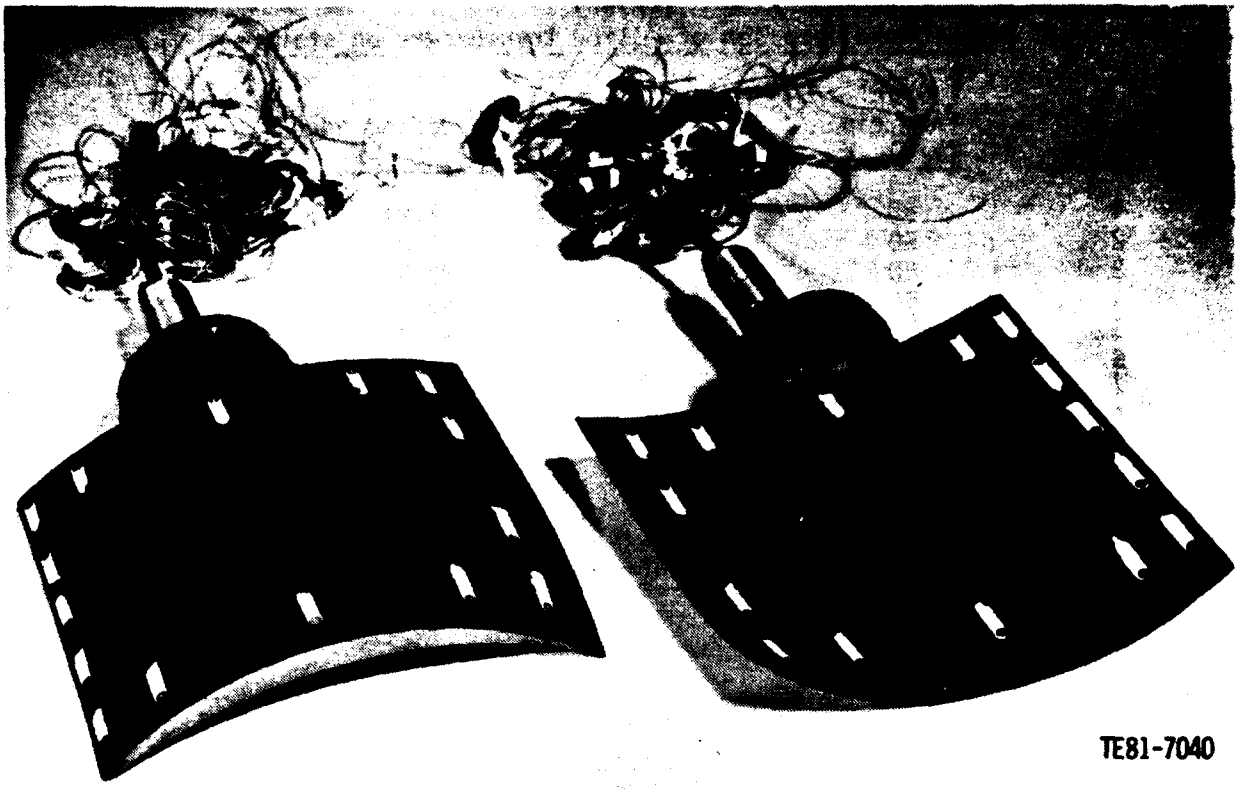

Figure 5. Radial and chordwise suction and pressure surface transducer instrument locations.

Calibration of the steady-stage pressure measuring system is accomplished automatically and on line. A deadweight system provides reference pressures of 0, 0.5, and 1.0 psia to the Scanivalve transducers. When the computer reads these pressures, a linear curve fit is used to establish a calibration curve for each of the six transducers. Then the data channels are interpreted, based on the proper curve. For time-variant pressures, the instrumented strators were placed in a pressure chamber, and five levels of pressure, ranging from 8 psia to slightly above ambient, were used to construct a calibration curve for each of the installed transducers. These curves were read into the computer for transducer voltage conversions to pressure.

Table 3.
Axial chord location of Kulite transducers on stators.

Kulite No.	Span from tip (z/ℓ)--%	From leading edge (x/C)--%	
1	50	2.94	
2	50	10.0	
3	50	20.0	
4	50	30.0	
5	50	40.0	
6	50	50.0	
7	50	60.0	
8	50	70.0	
9	50	80.0	
10	50	90.0	
11	50	97.0	
		Pressure surface	Suction surface
12	5.0	3.5	2.0
13	5.0	14.4	13.7
14	5.0	45.0	45.3
15	5.0	74.9	75.5
16	5.0	89.6	90.4
17	25.0	3.5	2.0
18	25.0	89.6	90.4
19	50.0	3.5	2.0
20	70.0	3.5	2.0
21	70.0	89.6	90.4
22	90.0	3.5	2.0
23	90.0	14.4	13.7
24	90.0	45.0	45.3
25	90.0	74.9	75.5
26	90.0	89.6	90.4

Calibration of the crossed-wire probe is obtained via a controlled temperature air jet capable of furnishing velocities over the range of interest. Data at standard temperature (room ambient) are obtained and represent a baseline velocity versus wire output voltage curve. This curve is linearized electronically using built-in features of the anemometry system. Corrections for temperature are made internally in the computer based on the temperature difference from the baseline value.

The data acquisition sequence is divided into three segments: steady-state performance, measurement of dynamic pressures, and measurement of wake velocity.

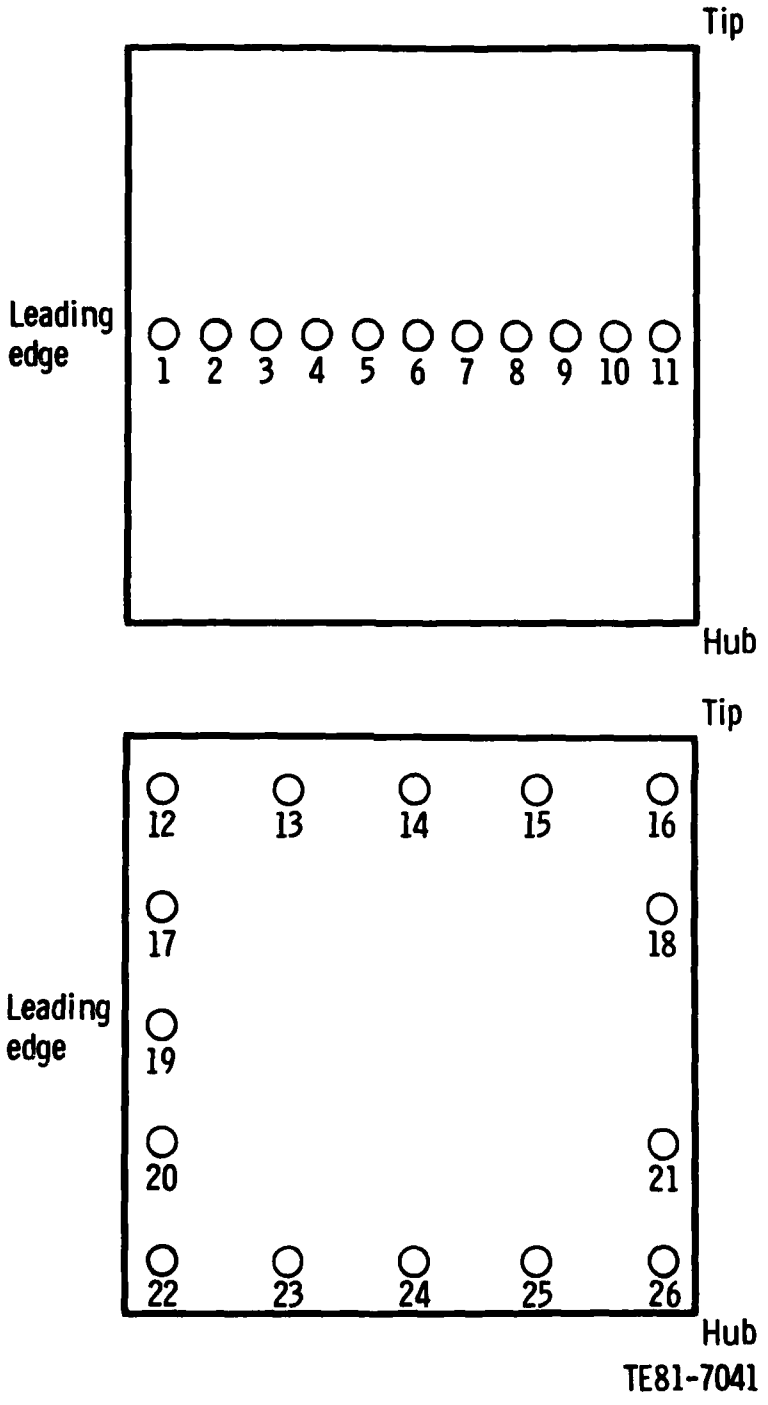

Figure 6. Location of Kulites on stator airfoils.

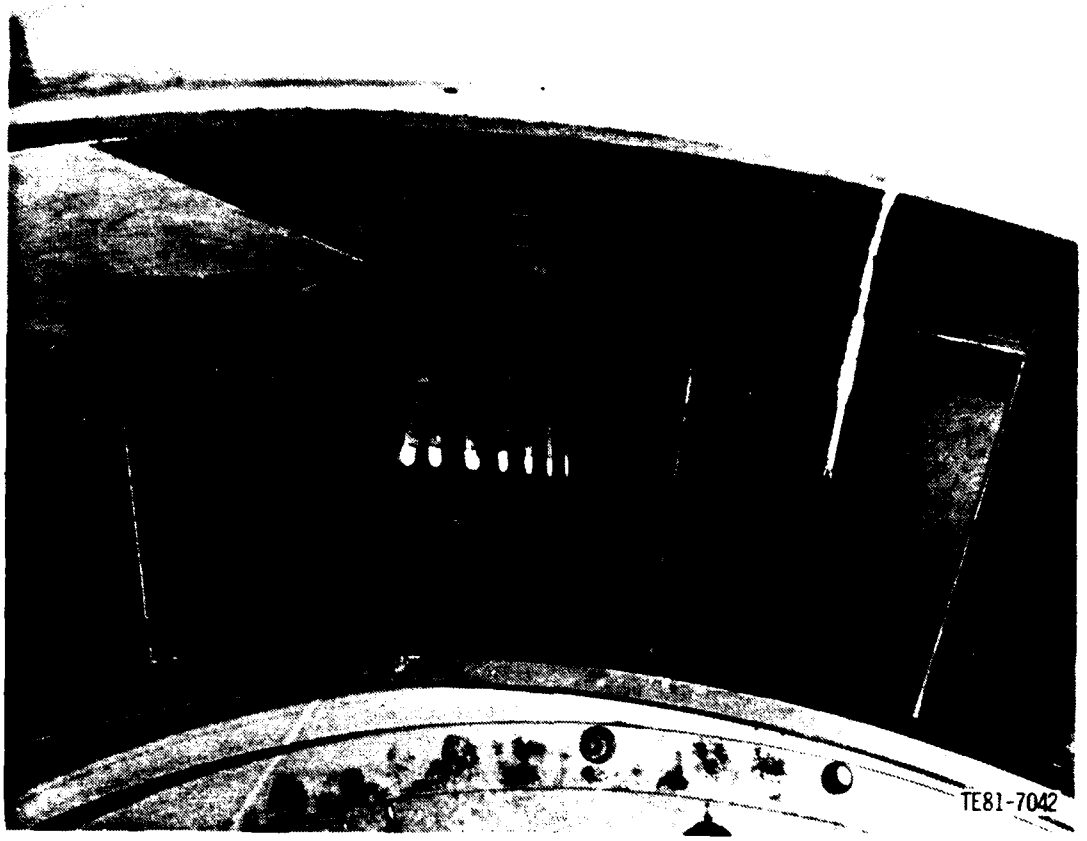

Figure 7. View of typical hot-wire installation in low speed compressor vane row.

The steady-state data acquisition follows the standard format of establishing corrected rotor speed and calculating pressure ratio, mass flow rate, and other compressor performance parameters.

Time-variant measurements of the airfoil surface pressures and rotor wakes require additional hardware and software to process the dynamic signals. An optical encoder, which delivers a positive 1.5-microsecond voltage spike during each rotor revolution, is used to trigger the Preston A/D converter. Each time the converter is triggered, data points are taken over a time period equal to the passage time of two rotor wakes. These data are stored in the computer in digital form, and the A/D trigger is reset by the computer. When the encoder voltage spike is recognized, another sample of data containing a number of

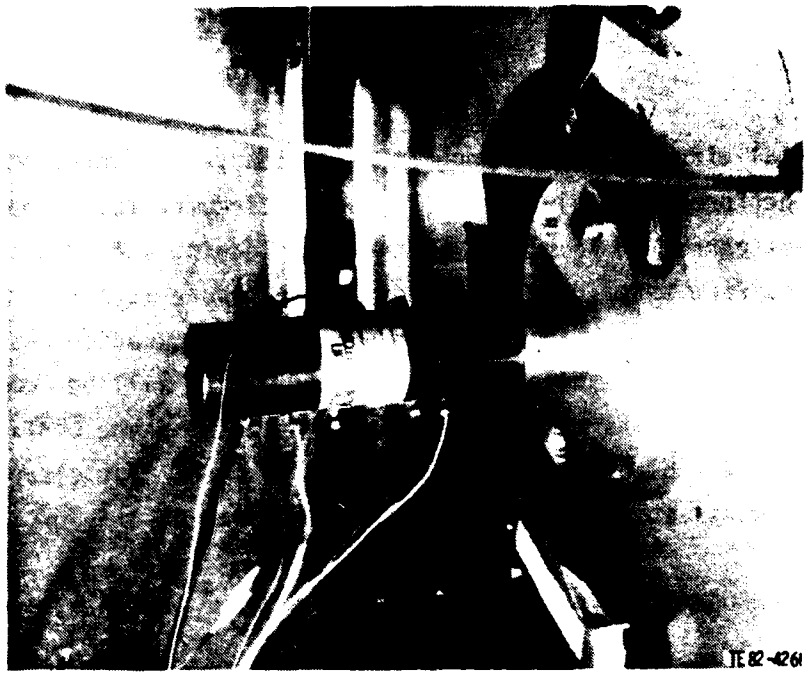

Figure 8. Meridian Laboratory 12-channel slip ring installed on the low speed compressor rotor face.

points identical to that of the first sample is acquired and stored. Three hundred of these samples (ensembles) are acquired and stored for each data sequence.

A computer retrieval algorithm is used to read the data from a disk storage location and to arrange the data according to transducer identification. The data ensembles are averaged in a point-to-point manner. Since each ensemble contains an identical number of points, the first point of each ensemble is averaged over the number of ensembles, followed by the second, etc, until all points have been averaged. This ensemble overlay improves the ability to distinguish signals occurring at blade passage frequency.

III. EXPERIMENTAL PROGRAM

The experimental effort for this program was conducted in three phases: (1) steady-stage performance evaluation, (2) radial/circumferential hot-wire anemometer surveys performed in planes at the vane leading and trailing edges, and (3) vane surface three-dimensional dynamic pressure measurement. As noted earlier, the blade tip clearance for the present configuration (BU 19) is 0.48% span. The experimental results for this configuration will be compared, where possible, with the results of Ref. 1 (BU 18) where the stage configuration was identical except the blade tip clearance was 3.0% span. The clearance under the vane hub was essentially zero for both configurations.

STEADY-STATE PERFORMANCE

The overall steady-state performance for the 0.48% span tip clearance configuration is illustrated in Figure 9. Also indicated on the figure are the 3.0% span tip clearance results from BU 18. The reduction in tip clearance produced an increase in flow, pressure ratio, and stall margin.

Four steady-state operating conditions were selected at which to acquire and evaluate the hot-wire anemometry and surface Kulite dynamic pressure signals. Those points were the same as the ones selected for the 3% span tip clearance investigations:

Data Point	
1	Open throttle
2	Intermediate
3	Near design
4	Near stall

Data point (DP) 1 represents the open throttle, maximum flow-rate/minimum pressure condition at design speed. DP 2 is a point in between the open throttle and design flow conditions. DP 3 represents the design conditions while DP 4 is a point between design and stalling conditions.

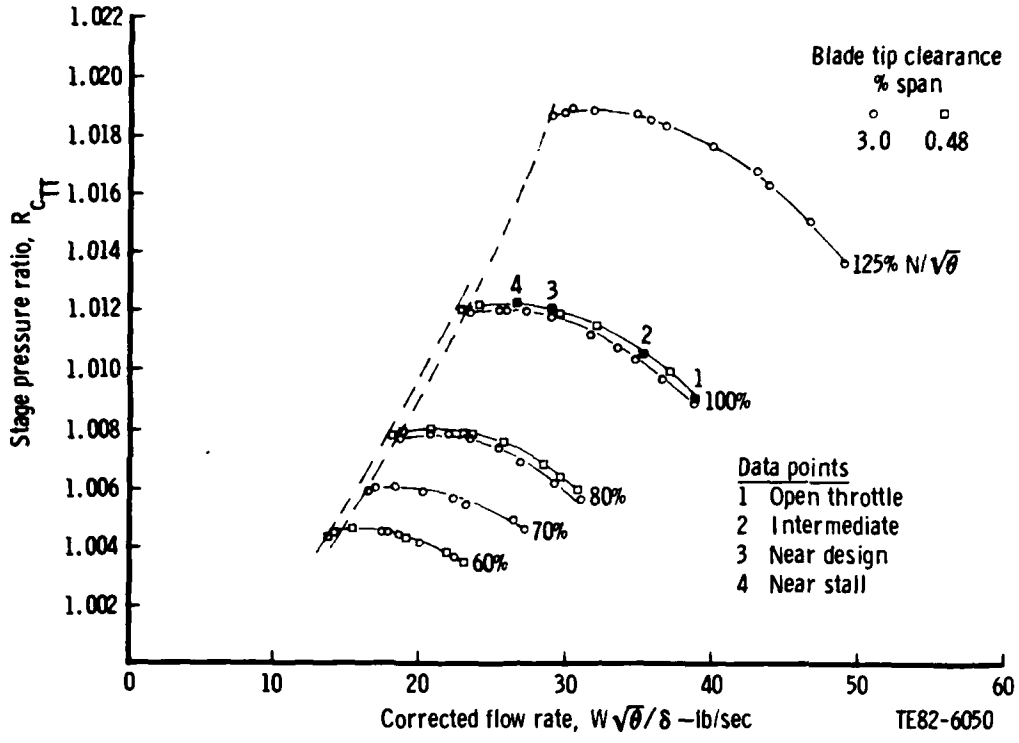

Figure 9. Effect of blade tip clearance on overall stage pressure ratio/flow rate characteristics.

At each of the four data points noted in Figure 9, the following measurements were made:

- o steady-state pressures and temperatures throughout the stage
- o hot-wire anemometry wake measurements at various radial/circumferential locations at the vane leading and trailing edge planes
- o dynamic pressure measurements from 52 Kulite gages on the vane airfoil surface
- o dynamic pressure measurements from the two Kulite gages on the rotor tip section trailing edge

BLADE TIP SECTION TRAILING EDGE DYNAMIC PRESSURE RESULTS

Rotor blade tip section trailing edge Kulite signals were processed for the four selected steady-state operating points. The results of the magnitude and phase lag relationships, as a function of stage loading from open throttle to stall, are shown in Figure 10. The results indicate that these suction and

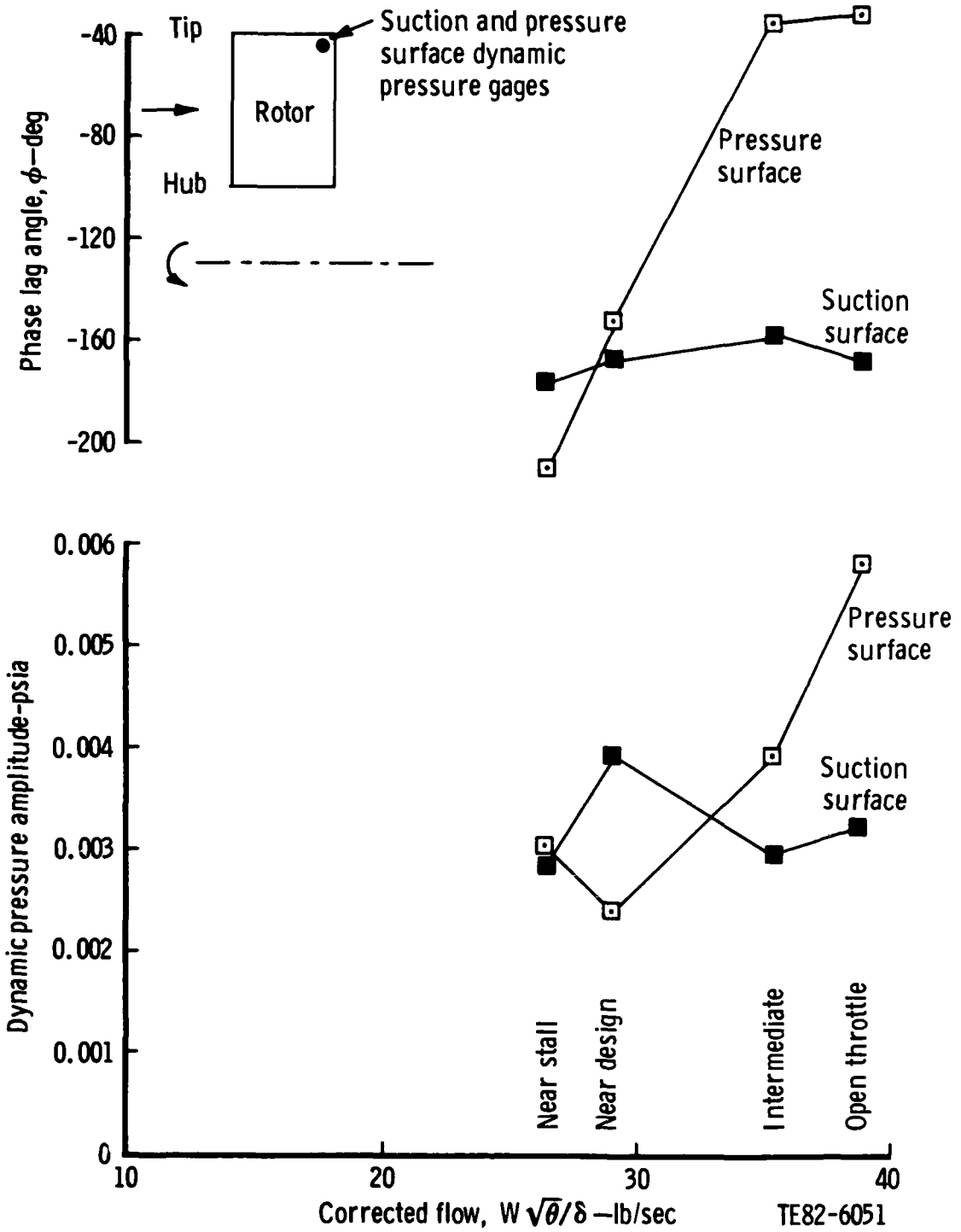

Figure 10. Rotor tip section trailing edge dynamic pressure and phase lag variation with stage operating conditions, 100% speed, 0.48% span blade tip clearance.

pressure surface trailing edge dynamic signals come into phase with each other as the design operating conditions are approached. The results also show that at open throttle conditions the magnitude of the dynamic pressure was largest on the pressure surface, but the values on the two airfoil surfaces approached the same magnitude as the stage was back-pressured toward stall.

VANE INLET CONDITIONS

At each of the four selected steady-state operating points detailed, radial/circumferential hot-wire surveys were performed at the vane leading edge. This was done to establish (1) the three-dimensionality of both the steady and dynamic flow fields entering the vane and (2) the radial distribution of the magnitude and phase character of the transverse fluctuating velocity component of the vane inlet flow field. The transverse fluctuating velocity component is a measure of the unsteady blade wake defect and correlates directly with the magnitude of the unsteady pressure induced at the vane leading edge.

Contour plots of steady and dynamic velocities, air angles, and phase angles are presented in Figures 11 through 16 for the rig operating at near-design conditions. Contour plots of these parameters have similar shape and characteristics at other selected operating points and will not be presented here.

Figure 11 presents the vane inlet absolute velocity field. Near-design conditions are essentially established in the outer two-thirds of the airfoil. Casing endwall boundary layer effects are apparent in the tip region flow field. In the inner one-third span region the velocity level increases as the hub wall is approached. This was due to overcambering with subsequent overpressuring by the rotor. The presence of the vanes, as noted by the vane leading edge locations in Figure 11, exerts a strong influence on the leading edge plane velocity field. At all radial locations, except near the tip endwall where boundary layer effects dominate, the flow decelerates as the vane leading edge is approached in the circumferential direction.

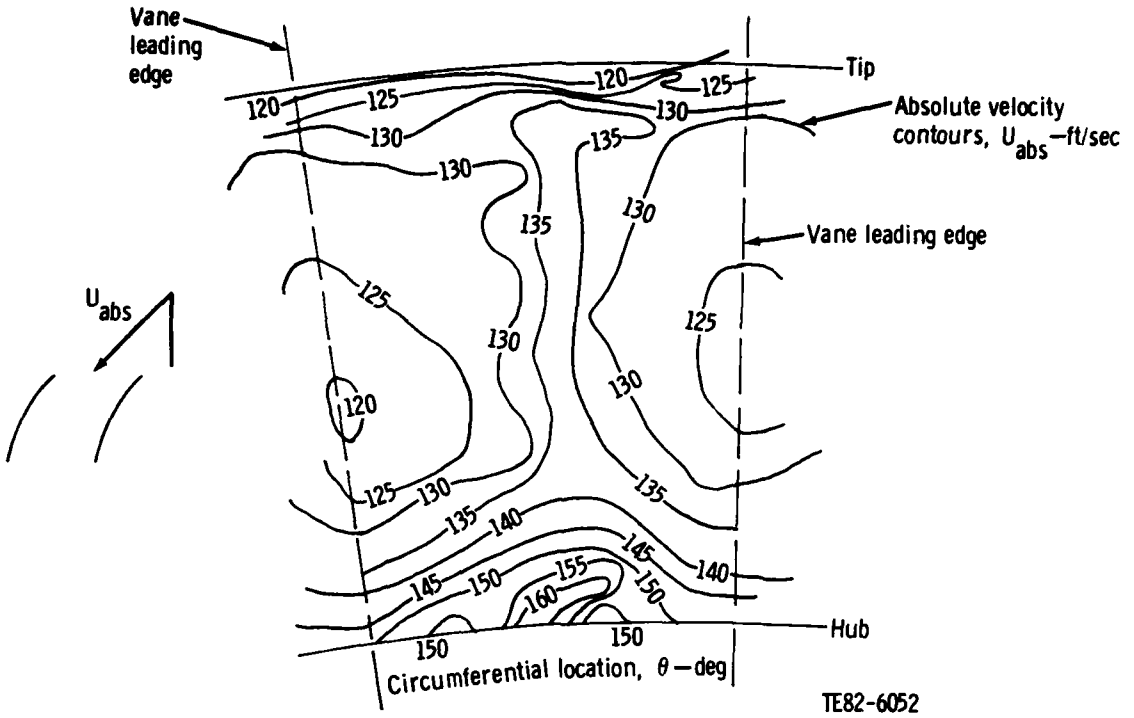

Figure 11. Vane leading edge absolute velocity contours at near-design operating conditions, 0.48% span blade tip clearance.

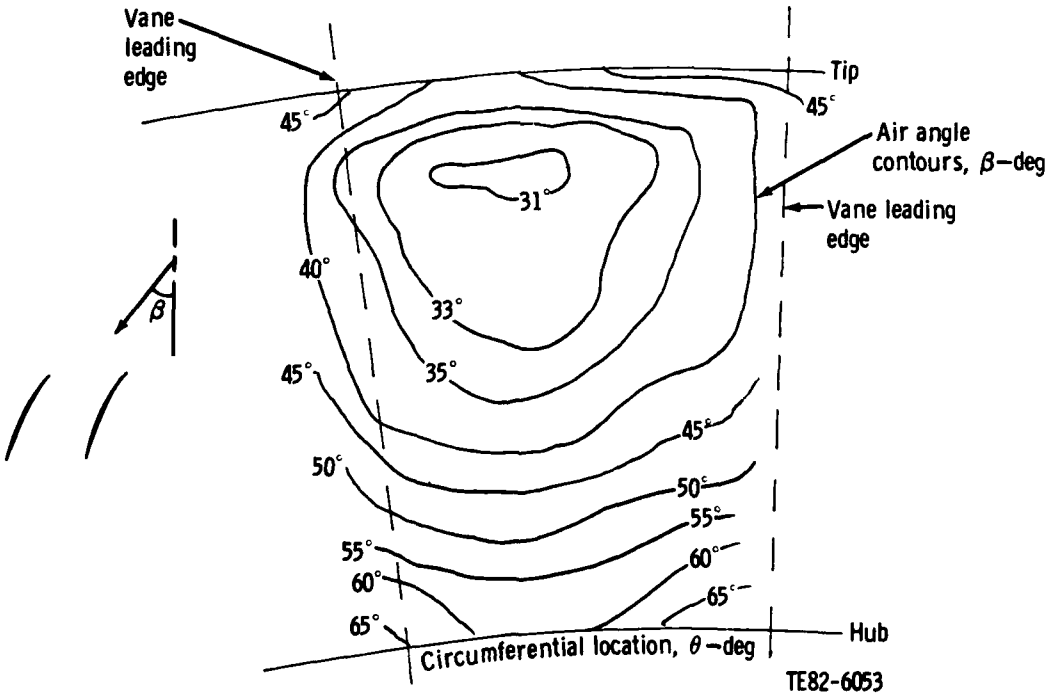

Figure 12. Vane leading edge air angle contours at near-design operating conditions, 0.48% span blade tip clearance.

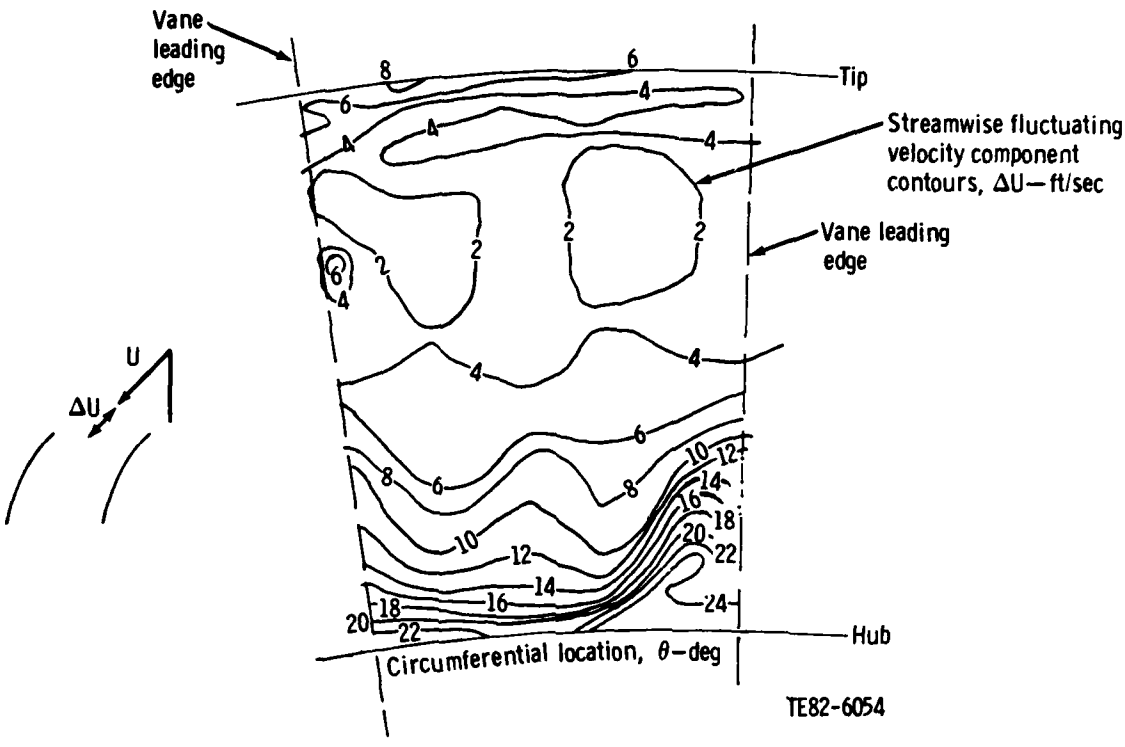

Figure 13. Vane leading edge streamwise fluctuating velocity component ΔU at near-design operating conditions, 0.48% span blade tip clearance.

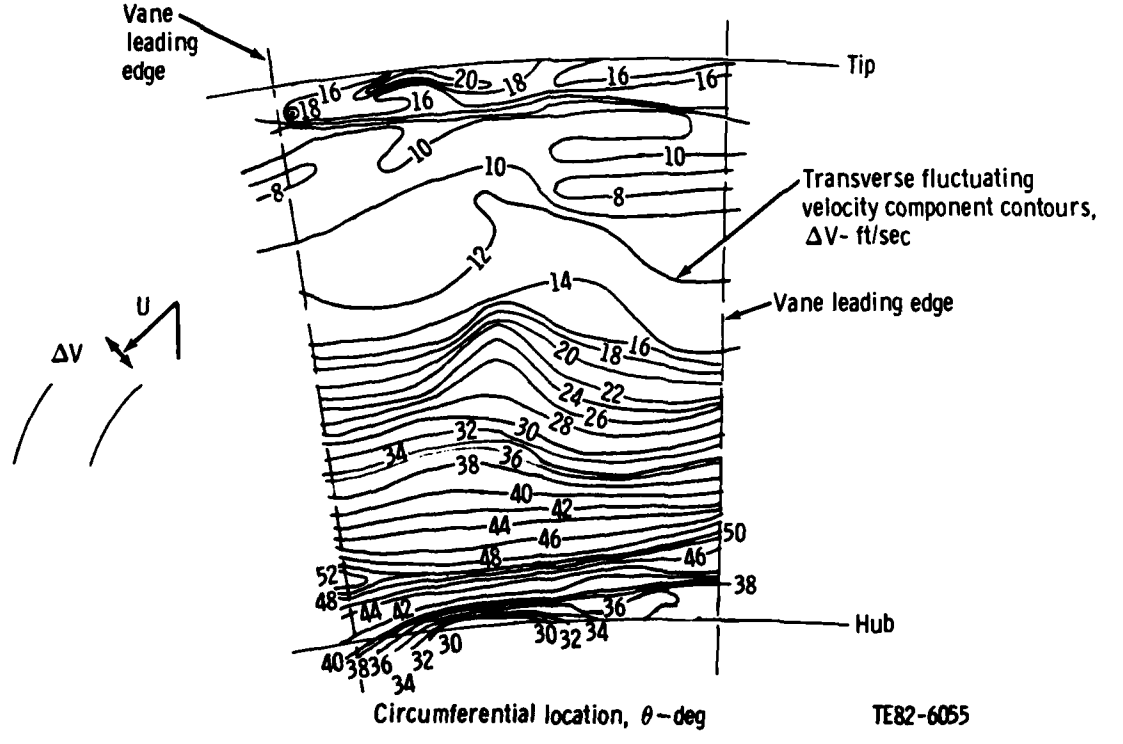

Figure 14. Vane leading edge transverse fluctuating velocity component ΔV at near-design operating conditions, 0.48% span blade tip clearance.

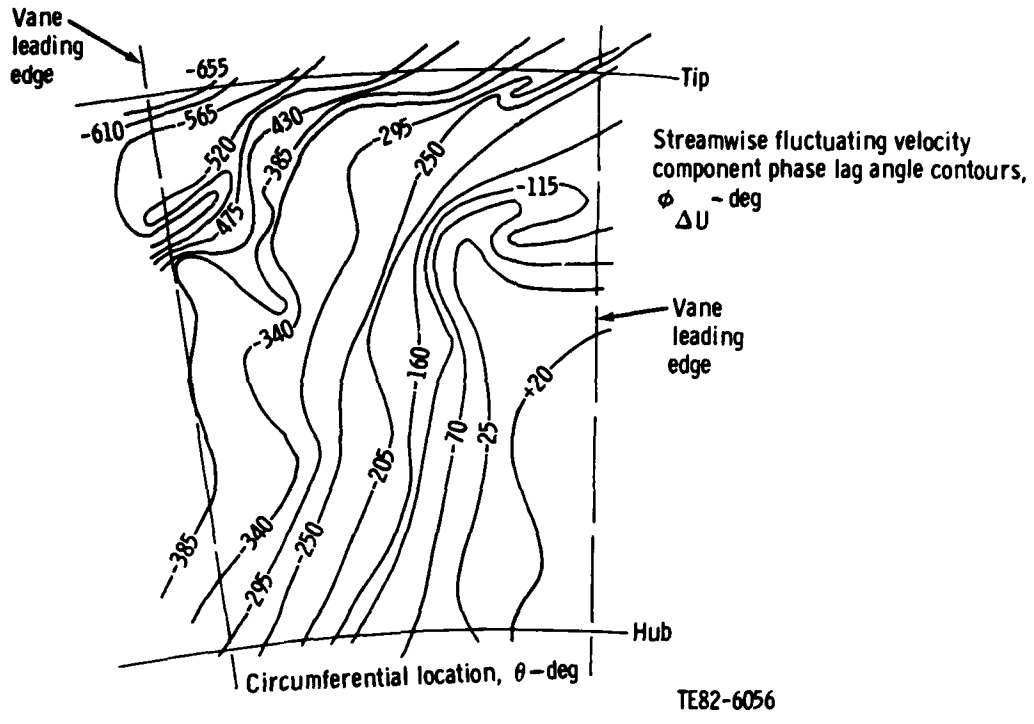

Figure 15. Vane leading edge streamwise fluctuating velocity component phase lag angle at near-design operating conditions, 0.48% span blade tip clearance.

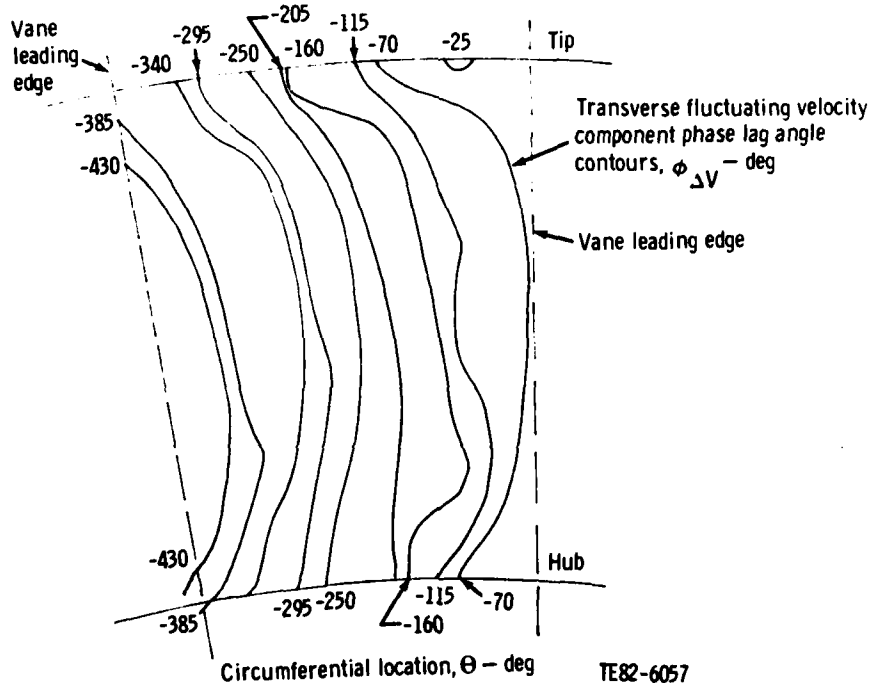

Figure 16. Vane leading edge transverse fluctuating velocity component phase lag angle at near-design operating conditions, 0.48% span blade tip clearance.

Vane inlet angle contours are illustrated in Figure 12. Again, large changes are noted as both the hub and the tip endwalls are approached. The presence of the vane leading edges also results in an increase in air angle as the vane is approached in the circumferential direction.

Figures 13 and 14 show, respectively, the distribution of the streamwise and transverse fluctuating velocity component magnitudes in the radial and circumferential directions. These components are the result of the velocity defect of the blade wake that passes the vane leading edge.

Figures 11 through 16 show, in general, that both ΔU and ΔV are fairly uniform circumferentially. The exception to that can be noted in Figure 13, where there is a sharp gradient in ΔU in the vane leading edge hub region. Phase lag angles of the streamwise and transverse fluctuating velocity components are shown in Figures 15 and 16, respectively. All phase angles are measured relative to the encoder signal; and to be consistent with previous work of Ref. 1, all phase angles are considered as lagging (-) angles. Since the encoder triggered the reference signal at precisely the same time for each rotor revolution, the phase angle is a measure of time for the disturbance signal (wake defect) to move from one position to another. For example, Figures 15 and 16 show that in the neighborhood of one vane leading edge the phase lag angle was around zero, while it was approximately 400 deg at the next vane in the counterclockwise direction. That is, the disturbance signal moved past one vane leading edge about 400 deg after it had passed its clockwise neighbor. Figures 15 and 16 show that the inner two-thirds span of $\phi_{\Delta U}$ and all of $\phi_{\Delta V}$ are essentially independent of radial position. $\phi_{\Delta U}$ is, however, strongly influenced by the tip endwall and the presence of the vane leading edges in the outer one-third span of the vane passage.

Figures 17 and 18 show the radial distribution of nondimensionalized $\Delta V/U_{abs}$ and its phase angle in the vane leading edge plane midway between vanes. Those figures also show (1) the influence of stage loading and (2), by way of the Ref. 1 results, the impact of blade tip clearance on $\Delta V/U_{abs}$ and $\phi_{\Delta V}$. In general, the disturbance quantity, $\Delta V/U_{abs}$ increased with increased loading, having the largest values in the endwall regions. Although there was some radial redistribution, with the exception of the near-stall condition, the reduced

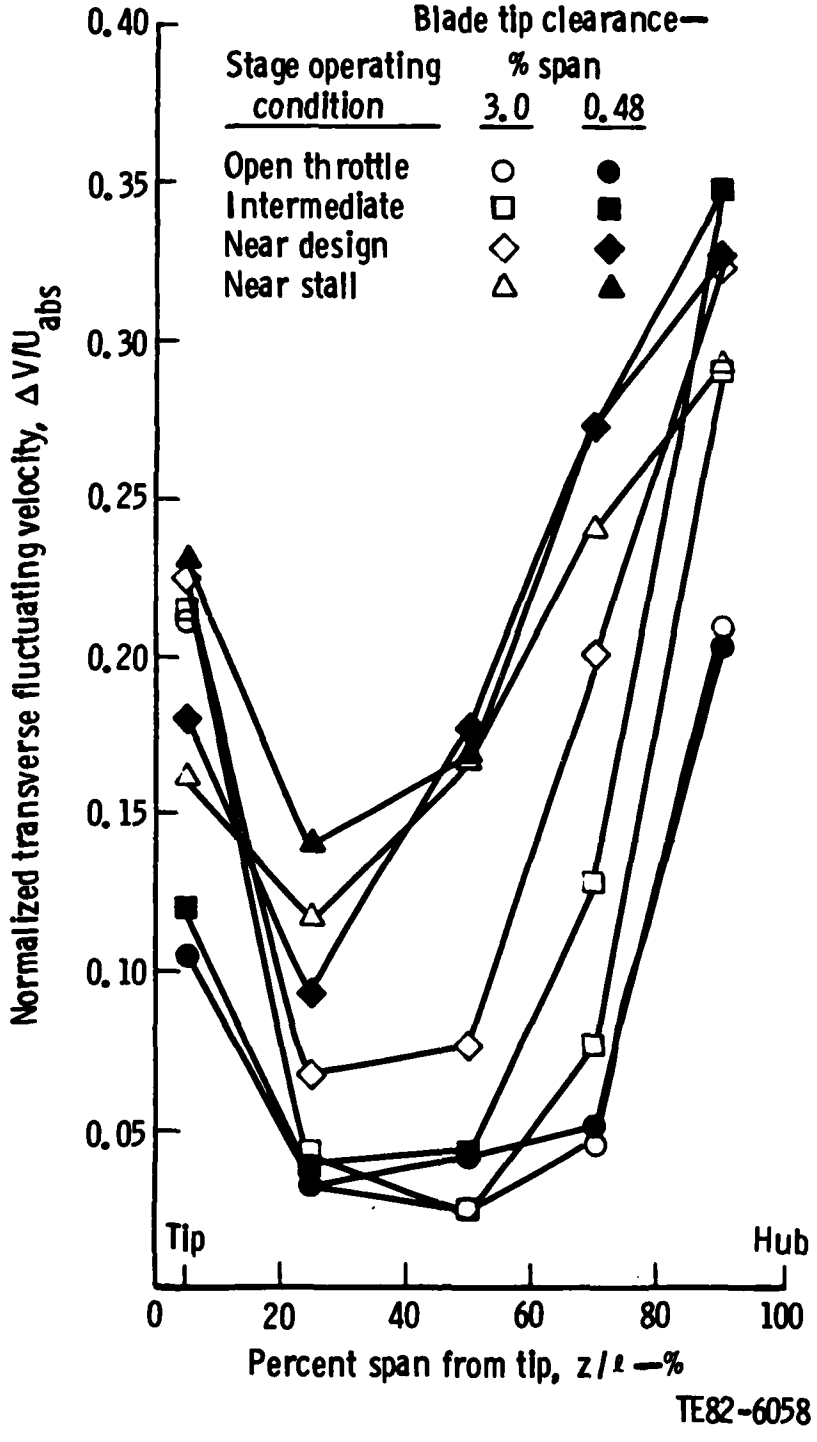

Figure 17. Influence of blade tip clearance on normalized transverse fluctuating velocity component at vane inlet midpassage, 100% speed.

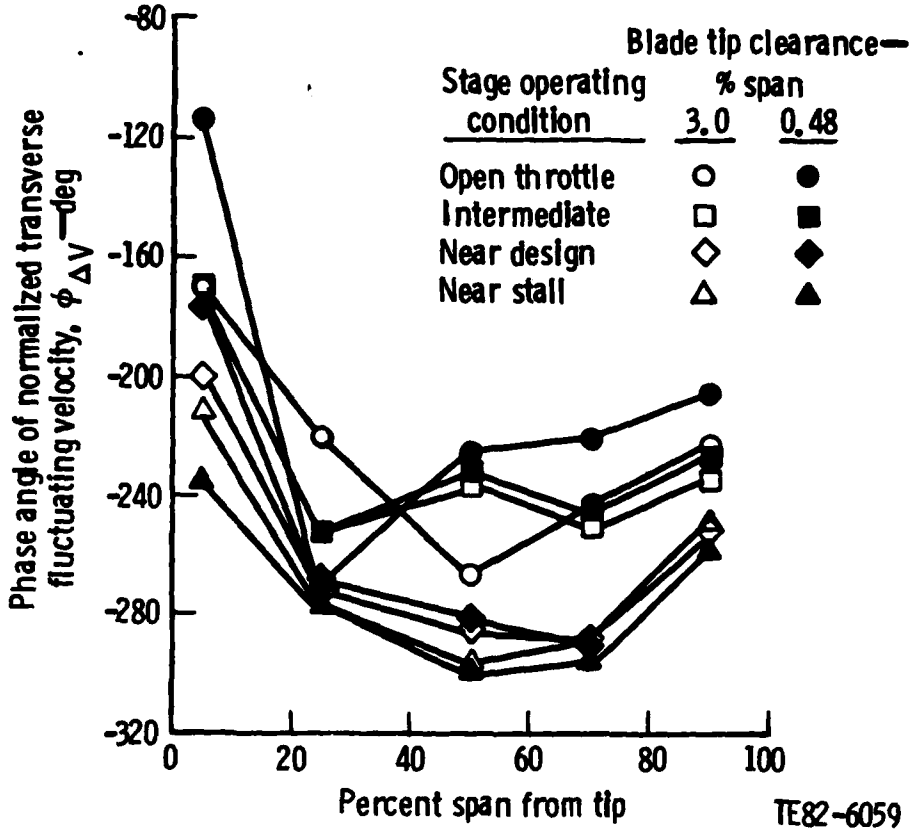

Figure 18. Influence of blade tip clearance on phase angle of the normalized transverse fluctuating velocity component at vane inlet midpassage, 100% speed.

tip clearance produced a smaller value of $\Delta V/U_{abs}$ in the tip end region. Figure 18 also shows that the small blade tip clearance results produced a much larger variation and, generally, a reduced phase lag angle in comparison with the larger 3% span blade tip clearance results.

VANE SURFACE DYNAMIC PRESSURE RESULTS

Vane Surface Dynamic Pressure Magnitude

Dynamic pressure magnitude results for the near-tip section gages are presented in Figures 19, 20, and 21 for the 0.48% and 3.0% blade span tip clearance configurations. As shown in Figure 19, the dynamic pressure difference across the airfoil tip section was substantially reduced when the blade tip clearance and,

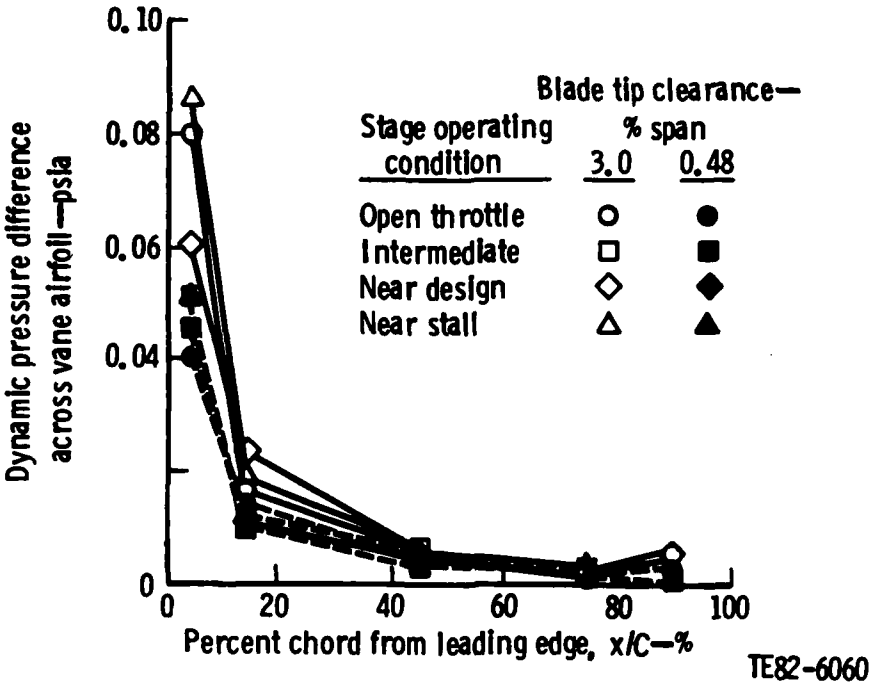

Figure 19. Influence of blade tip clearance on dynamic pressure differential across vane near-tip section, 100% speed.

hence, wake defect forcing function were reduced. For example, at the near-design operating condition the vane tip leading edge dynamic pressure difference was reduced 32% when the blade tip clearance was reduced from 3.0% to 0.48% span. Figures 20 and 21 illustrate that most of the dynamic pressure magnitude reduction was accomplished on the vane suction surface.

Figure 22 illustrates that a very slight influence of the blade tip clearance on the vane passage flow field was still present at the vane mean section. Continuing on to the hub region, Figure 23 shows that there was no discernible influence of the blade tip clearance on the vane hub region passage flow field. Figures 24 and 25 add additional support by illustrating that the gage response on both the hub section suction and pressure surfaces was unchanged by a significant reduction in blade tip clearance.

To further define how far radially inward the blade tip clearance effects penetrate, Figure 26 presents a radial distribution of the vane leading edge gage dynamic pressure response. In addition to the near-hub, mean, and near-tip

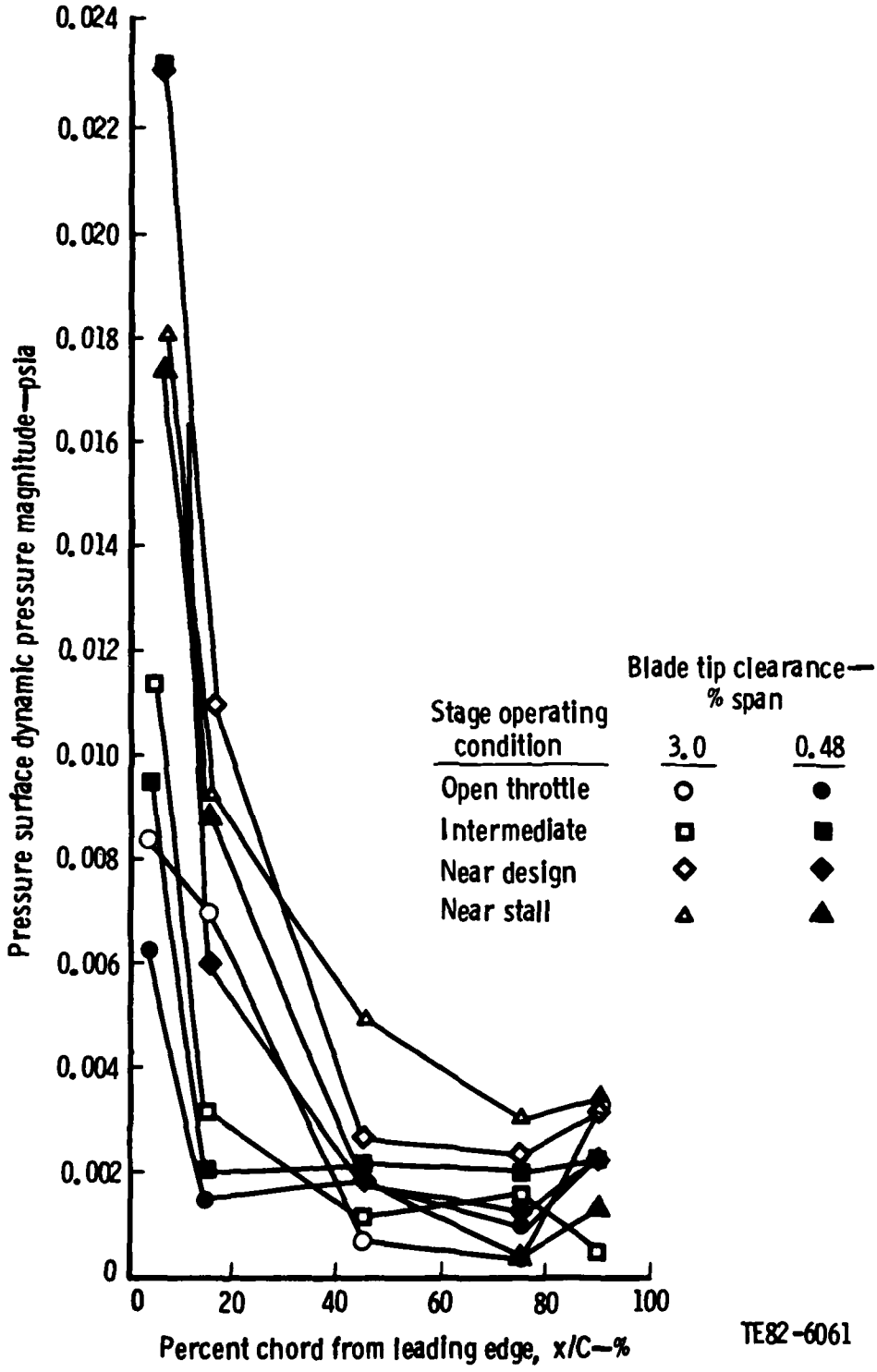

Figure 20. Influence of blade tip clearance on dynamic pressure magnitude on vane near-tip section pressure surface, 100% speed.

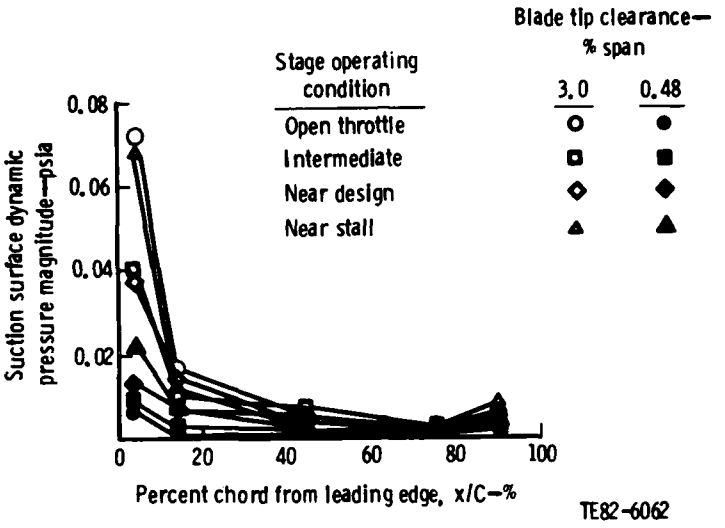

Figure 21. Influence of blade tip clearance on dynamic pressure magnitude on vane near-tip suction surface, 100% speed.

section data, gage response information was acquired at the 20% and 70% from tip section span locations. The illustration shows that the blade tip clearance effects were quite evident at the 20% from tip span location. A slight effect is evident at the mean section. Figures 27 and 28 document that along the leading edge, the influence of blade tip clearance on the dynamic pressure flow field shows up principally as a reduction in dynamic pressure response on the suction surface. The leading edge pressure surface was only slightly affected.

Gust analysis procedures such as those described in Refs. 3 and 4 employ the so-called strip assumption. That is, disturbance effects are assumed not to migrate radially as the disturbance propagates downstream. The present results show that for the large blade tip clearance configuration (i.e., 3.0% span) a significant radial migration took place. Therefore, for large clearance configurations, the gust analysis should probably be limited to analyzing airfoil mean sections.

It is of interest to highlight how far into the vane passage the blade tip clearance effects penetrate. The dynamic pressure difference across the vane trailing edge is presented in Figure 29. Although the signal strength is

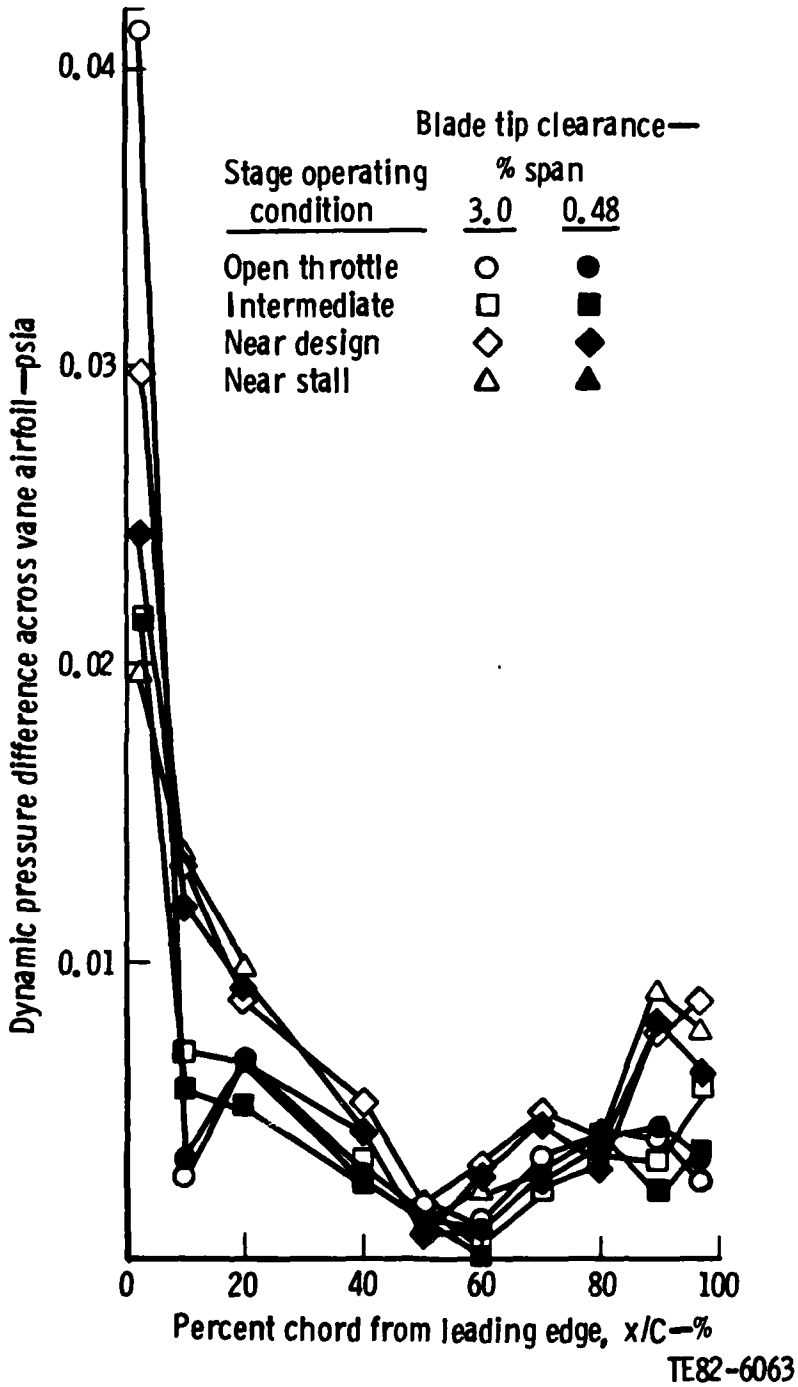

Figure 22. Influence of blade tip clearance on dynamic pressure differential across vane mean section, 100% speed.

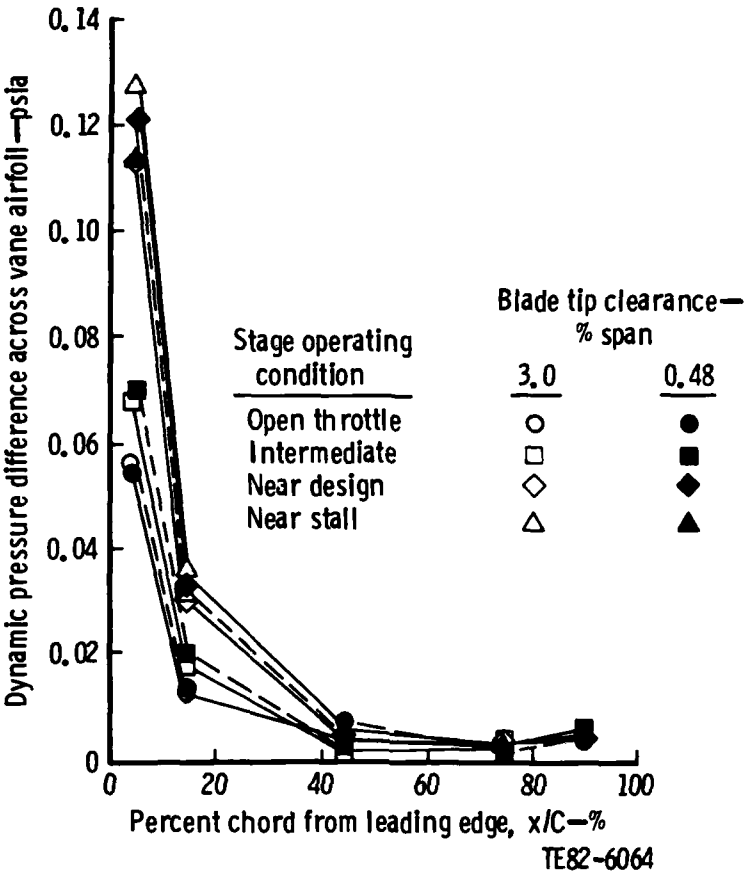

Figure 23. Influence of blade tip clearance on dynamic pressure differential across vane near-hub section, 100% speed.

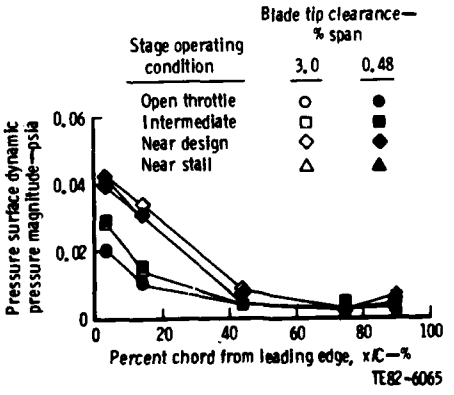

Figure 24. Influence of blade tip clearance on vane near-hub pressure surface dynamic pressure magnitude, 100% speed.

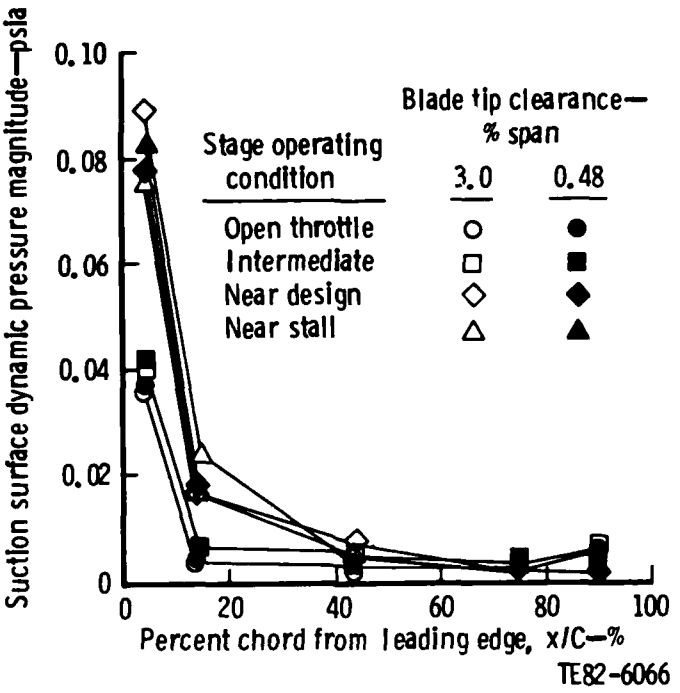

Figure 25. Influence of blade tip clearance on vane near-hub suction surface dynamic pressure magnitude, 100% speed.

quite small, Figure 29 does indicate that a reduction in blade tip clearance can effect a reduction in the vane trailing edge dynamic pressure response from the tip section down to at least the mean section.

Vane Surface Phase Lag Angle

The phase lag angle (measured relative to the encoder trigger signal) of the dynamic pressure difference across the vane at the tip, mean, and hub sections is shown in Figures 30, 31, and 32. These results indicate that, in general, the reduction in blade tip clearance produced a reduction in the phase lag angle at the tip section. Considering the accuracy with which phase angle can be determined, Figures 31 and 32 suggest no impact of blade tip clearance effects on phase lag angle at the mean and hub sections. Worthy of note is the large change in phase lag angle between 40% and 50% chord at the mean section of Figure 31. The phase angle variation is present in both the 3.0% and the 0.48% span blade tip clearance data. A rational explanation for this abrupt change in phase angle does not exist, and it is not predictable by present an-

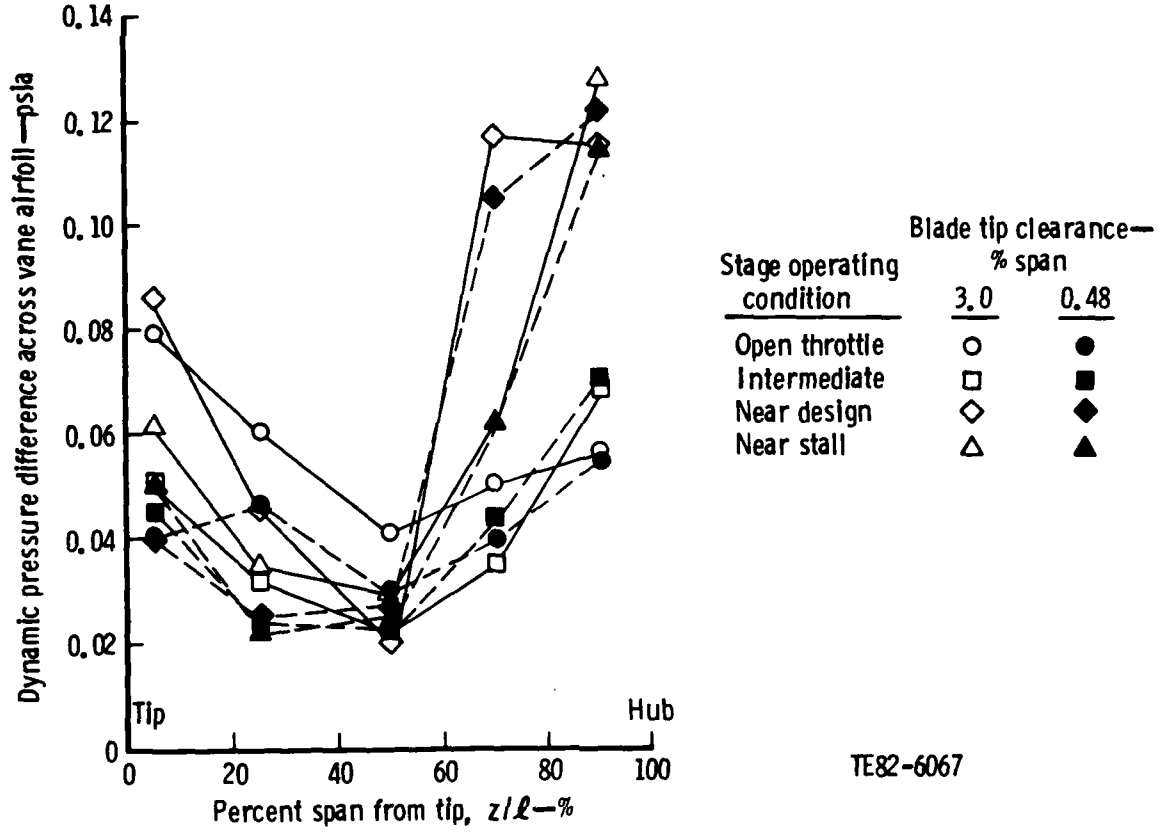

Figure 26. Influence of blade tip clearance on dynamic pressure differential across vane leading edge, 100% speed.

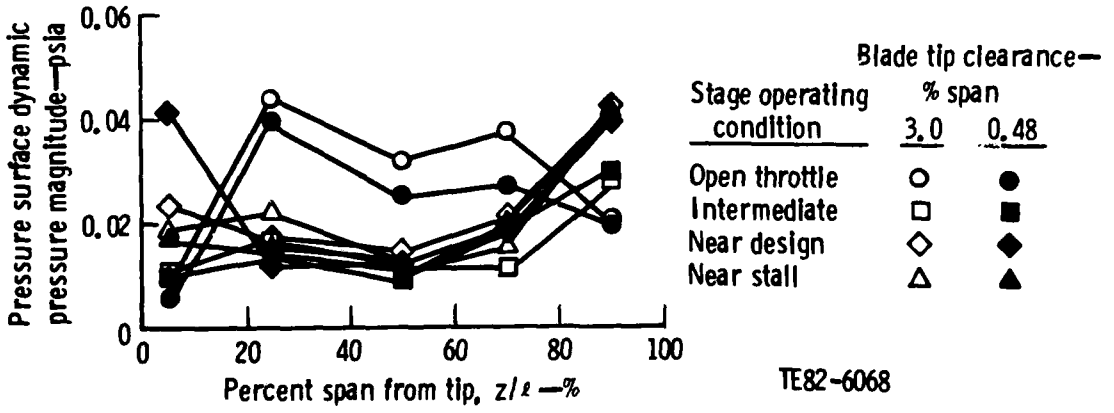

Figure 27. Influence of blade tip clearance on dynamic pressure magnitude on vane leading edge pressure surface, 100% speed.

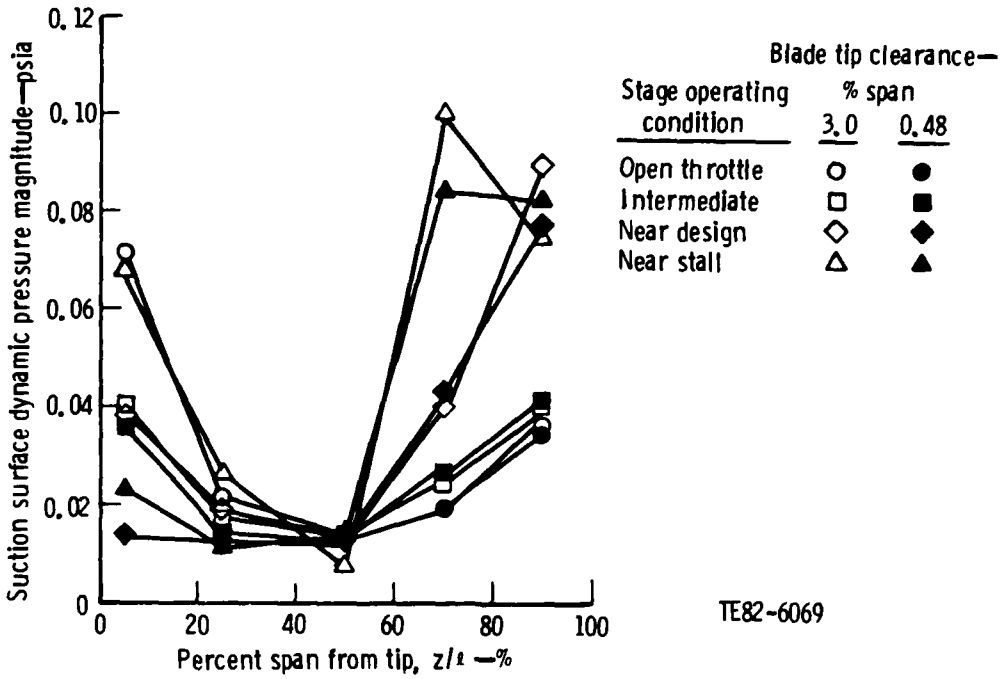

Figure 28. Influence of blade tip clearance on dynamic pressure magnitude on vane leading edge suction surface, 100% speed.

alysis procedures (as was noted in Ref. 1). Vane leading edge phase lag data are presented in Figure 33 for the dynamic pressure difference across the airfoil and in Figures 34 and 35 for the suction and pressure surface details, respectively. Interestingly enough, there was no significant effect of blade tip clearance on phase lag angle at the leading edge. Figures 34 and 35 show perhaps a slight reduction in phase lag angle at the tip section but a slight increase at 20% span from the tip. These variations may be due to scatter in ability to accurately claculate phase angle. Figure 36 shows a reduction in dynamic pressure difference phase lag angle in the trailing edge tip region with a reduction in blade tip clearance. There were no discernible effects of tip clearance on phase lag angle at other radial locations along the trailing edge.

Vane Surface Pressure--Phase Contour Plots

The experimental information presented in the discussions above represents a quantitative description of the influence of blade tip clearance on the dynamic pressure and phase characteristics induced on a vane by a moving upstream

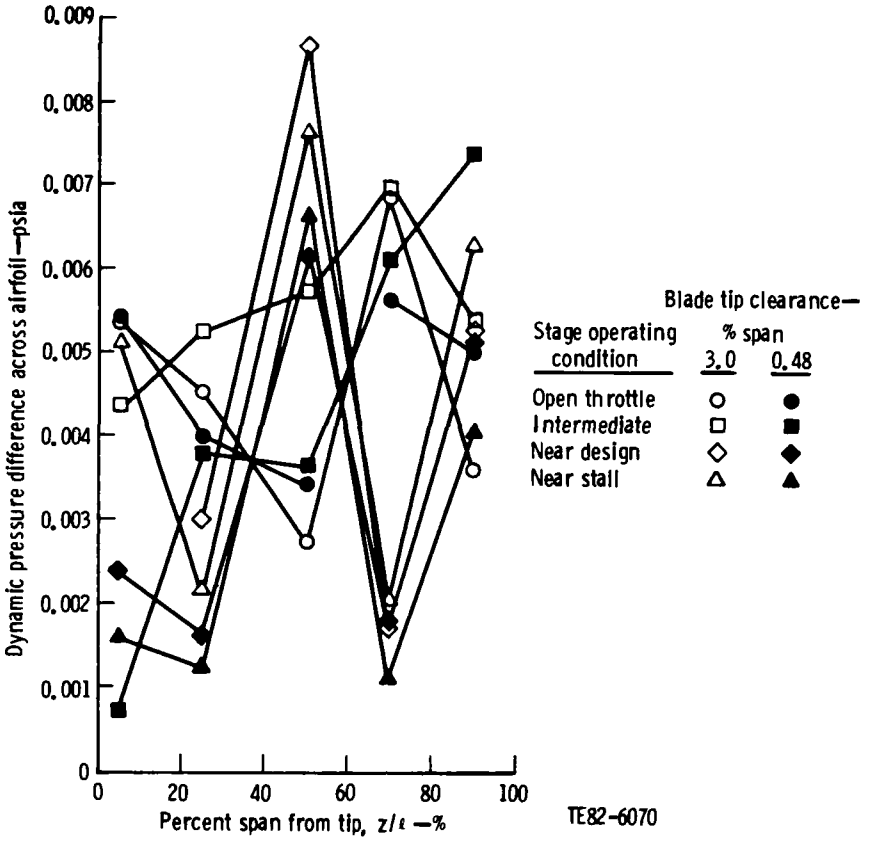

Figure 29. Influence of blade tip clearance on dynamic pressure differential at vane trailing edge, 100% speed.

rotor. However, those discussions have been limited to examining hub, mean, and tip sections, leading and trailing edge regions, etc, individually without being able to construct a picture of the dynamic pressure characteristic distribution over the complete vane airfoil. One data set was selected from which such a three-dimensional picture was constructed. The data point selected was the near-design operating point with the 0.48% span blade tip clearance configuration. Figure 37 presents a three-dimensional plot of the dynamic pressure on the entire vane surface by the upstream moving rotor. The vane is unwrapped about its leading edge. The first observation that is apparent is the large ridge of dynamic pressure at the vane leading edge. It has a minimum value at about two-thirds span from the hub, rising to a sharp peak at the tip and to a very large value in the hub region. The dynamic pressure falls away

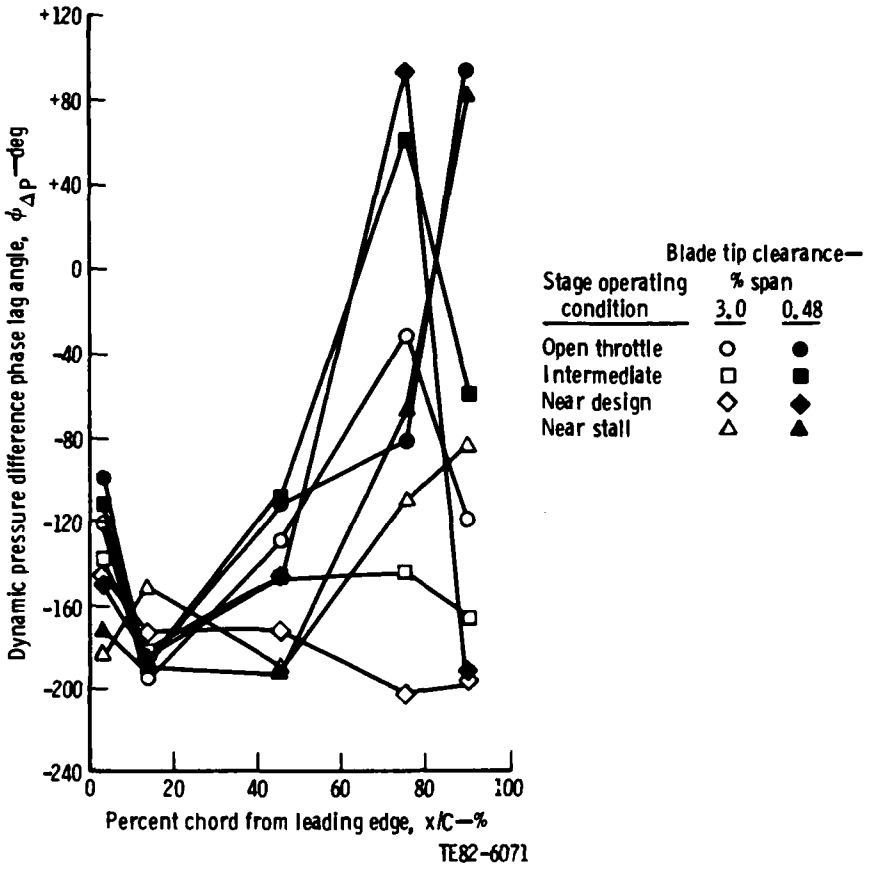

Figure 30. Influence of blade tip clearance on dynamic pressure differential phase lag angle at vane near-tip section, 100% speed.

rapidly, moving away from the leading edge, and then undulates over gentle hills and valleys as the trailing edge is approached. The dynamic pressure rises again at the trailing edge.

The wake defect forcing function at the tip is due to leakage flow through the tip clearance gap, the endwall boundary layer flow along the casing, and the blade trailing edge wake. (This will be made more clear by examining the oscilloscope traces in Figure 40.) Since (1) the operating point selected is near design and (2) a tip clearance of 0.48% span is a very small value, the tip section trailing edge wake defect is probably a minimum value and, therefore, the dynamic pressure response at the tip is also probably a minimum value. The huge magnitude of dynamic pressure in the hub region is due to the very poor flow conditions generated in the rotor hub region. Radial/circumferential hot wire survey results of Figures 11 and 12 shown earlier illu-

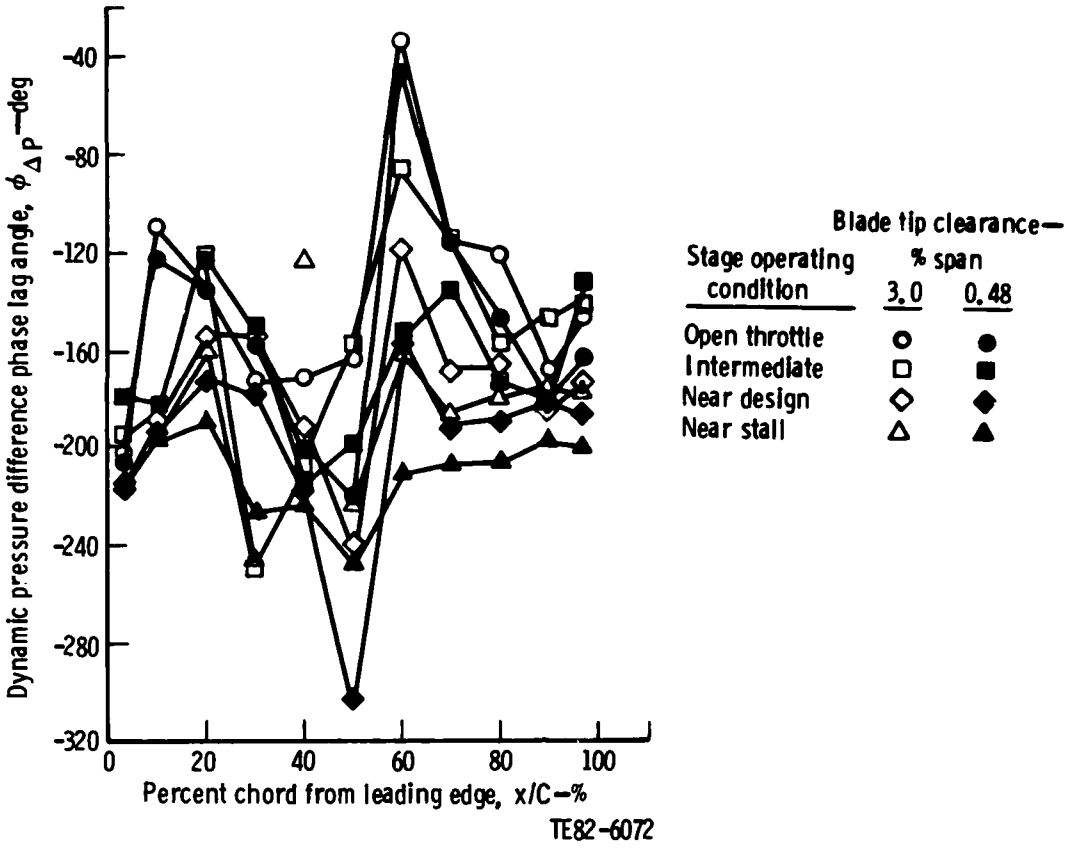

Figure 31. Influence of blade tip clearance on dynamic pressure differential phase lag angle at vane mean section, 100% speed.

strated high velocity and very large air angles with subsequent very large values of incidence angle implied on the vane leading edge in the inner one-third of the vane span. These conditions led to very large rotor hub wake defects (as will also be shown in Figure 40), which resulted in large values of induced dynamic pressure on the vane hub region leading edge.

A similar three-dimensional plot of phase lag angle distribution on the vane surface for the same stage operating condition was constructed and is presented in Figure 38. It may be noted there is not a strong radial influence on phase angle, but there are strong chordwise variations. For example, a phase difference of over 200 deg exists between the suction and pressure surfaces in

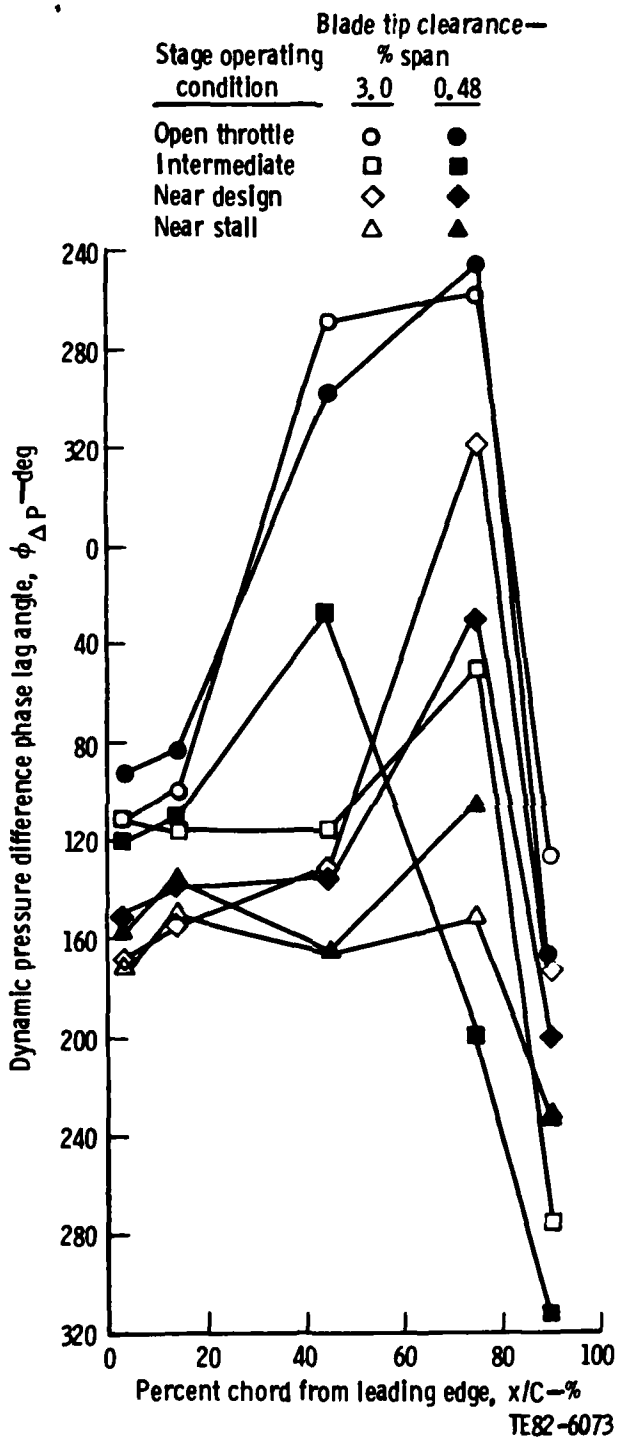

Figure 32. Influence of blade tip clearance on dynamic pressure differential phase lag angle at vane near-hub section, 100% speed.

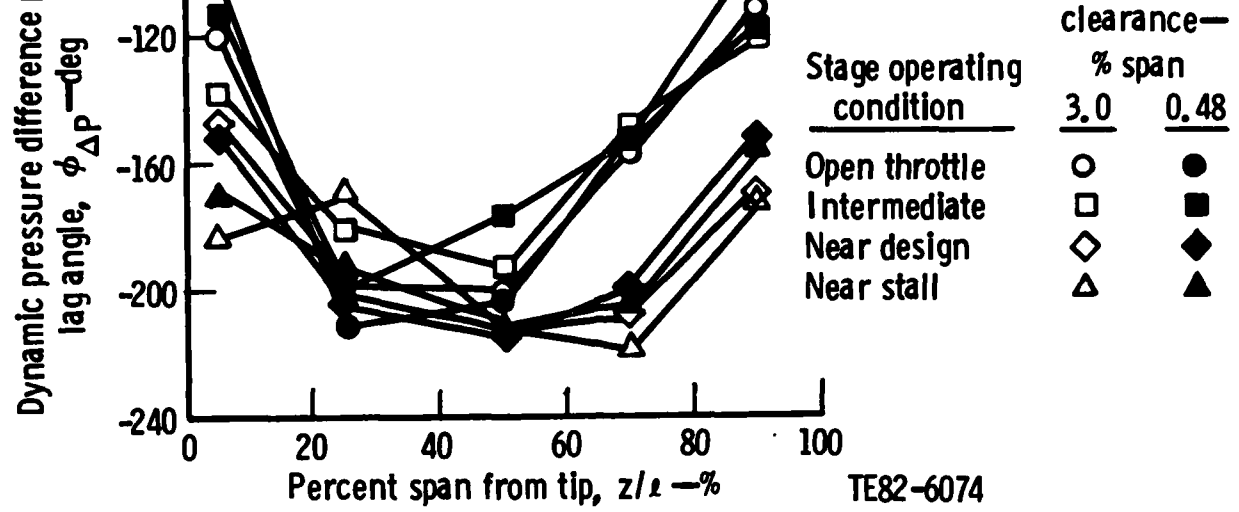

Figure 33. Influence of blade tip clearance on dynamic pressure differential phase lag angle at vane leading edge, 100% speed.

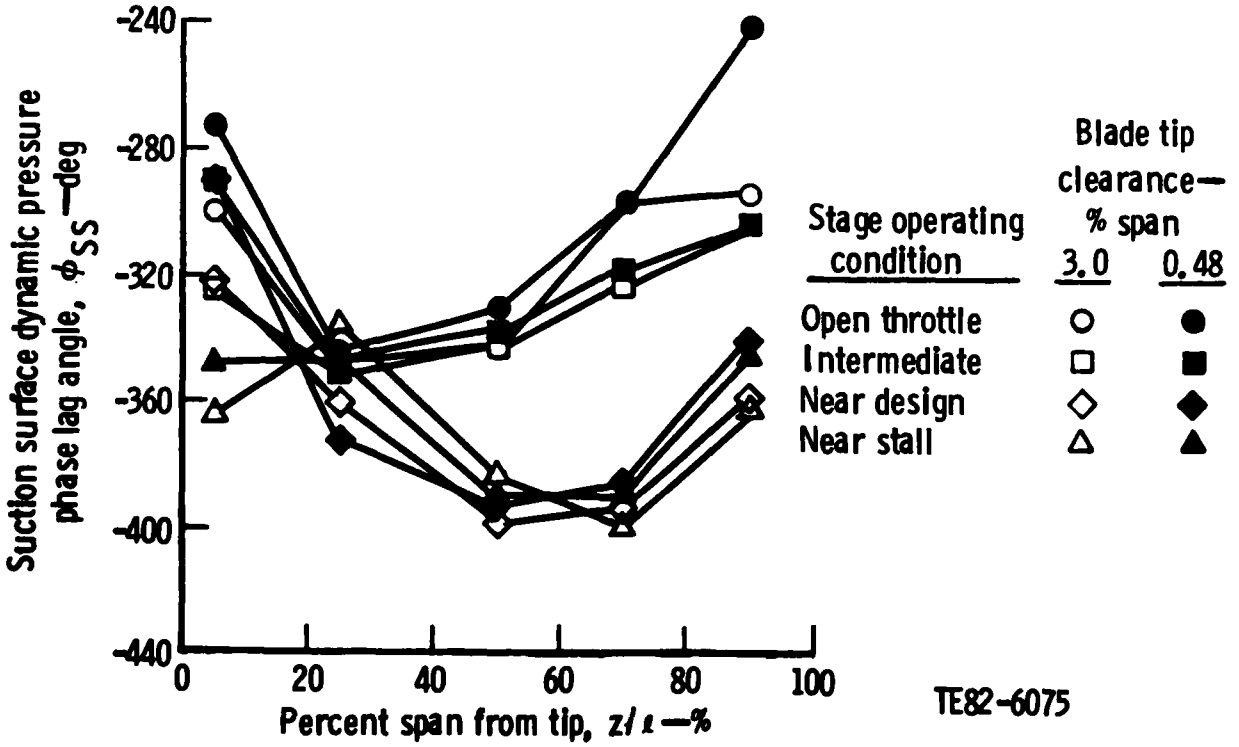

Figure 34. Influence of blade tip clearance on suction surface dynamic pressure phase lag angle at vane leading edge, 100% speed.

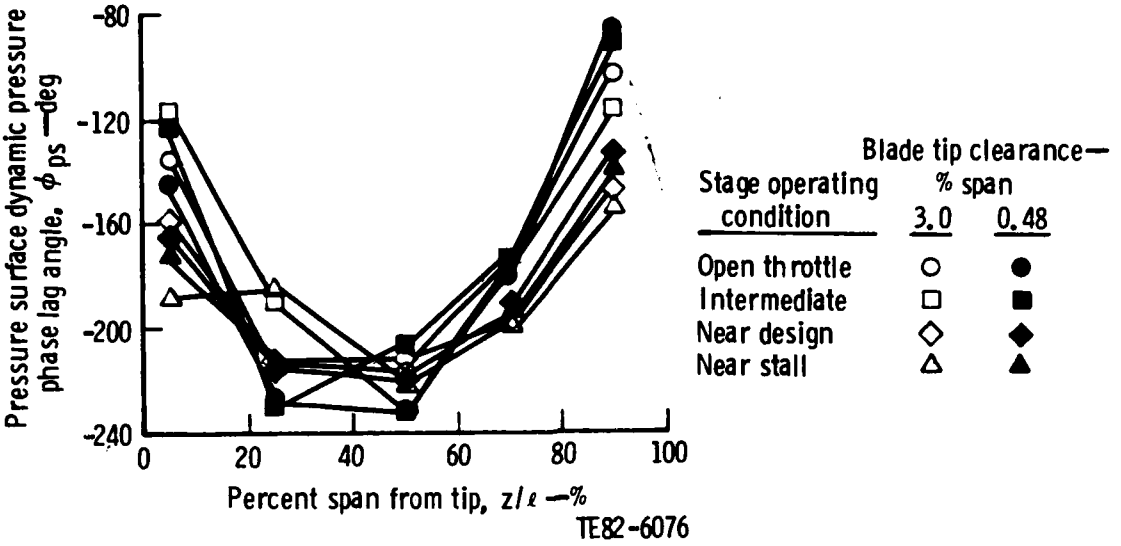

Figure 35. Influence of blade tip clearance on pressure surface dynamic pressure phase lag angle at vane leading edge, 100% speed.

the leading edge region. As one moves away from the leading edge, the two surfaces are nearly 180 deg out of phase until the 40%-50% chord location is reached. There, the phase lag angle on the suction surfaces changes abruptly to be essentially in phase with the pressure surface. The phase lag angle then increases again to its large negative value on the suction surface to be out of phase with the pressure surface values. This chordwise behavior of phase angle has been observed in all previous experiments with the stage hardware employed in the present investigation. The rapid change of suction surface phase lag angle at approximately 50% chord is not understood.

DYNAMIC SIGNAL OSCILLOSCOPE TRACES AND HARMONIC CONTENT

Each time a vane surface dynamic pressure or vane inlet and exit plane hot-wire signal was acquired for harmonic analysis, an oscilloscope trace record of that signal was also obtained. To help clarify where these data were taken refer to Figure 39. That illustration is an aft-looking-forward view of the vane passage showing the following:

- o Kulite gage locations
- o vane leading and trailing edge radial/circumferential planes
- o vane span dimensions
- o circumferential coordinates when radial hot-wire surveys were performed

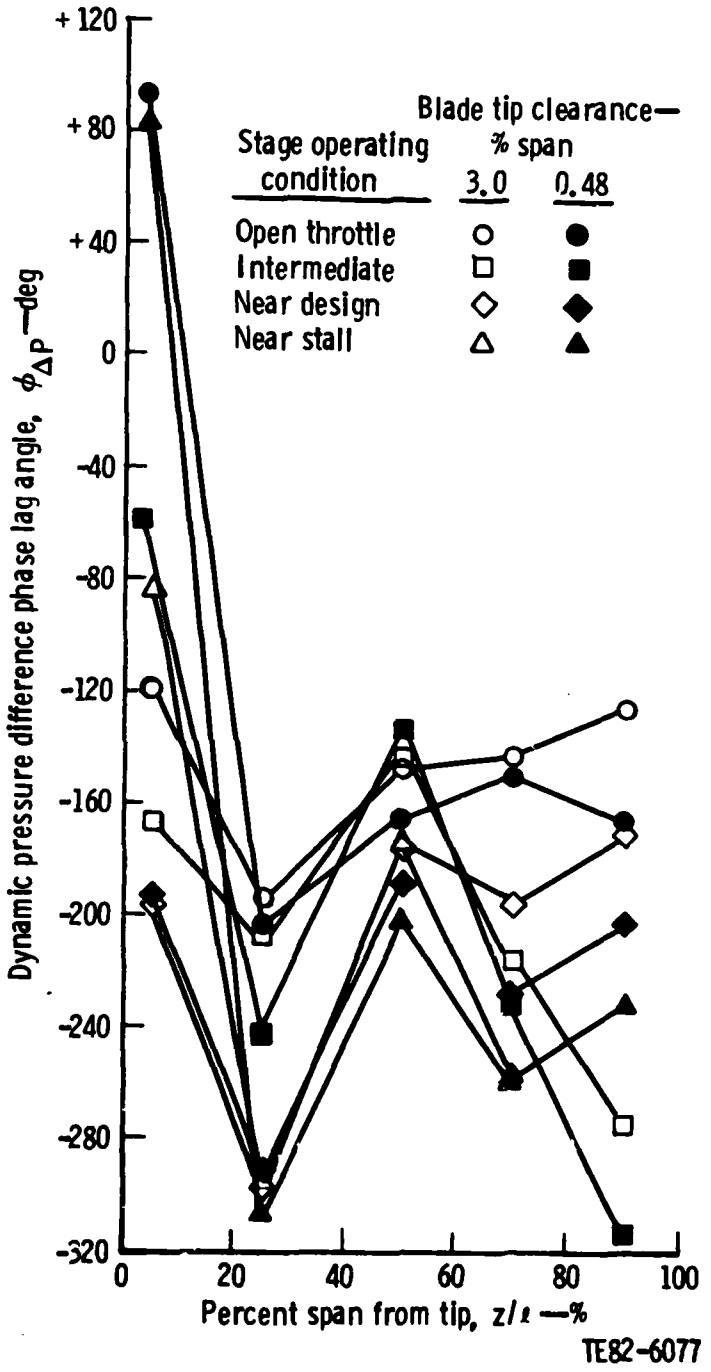

Figure 36. Influence of blade tip clearance on dynamic pressure differential phase lag angle at vane trailing edge, 100% speed.

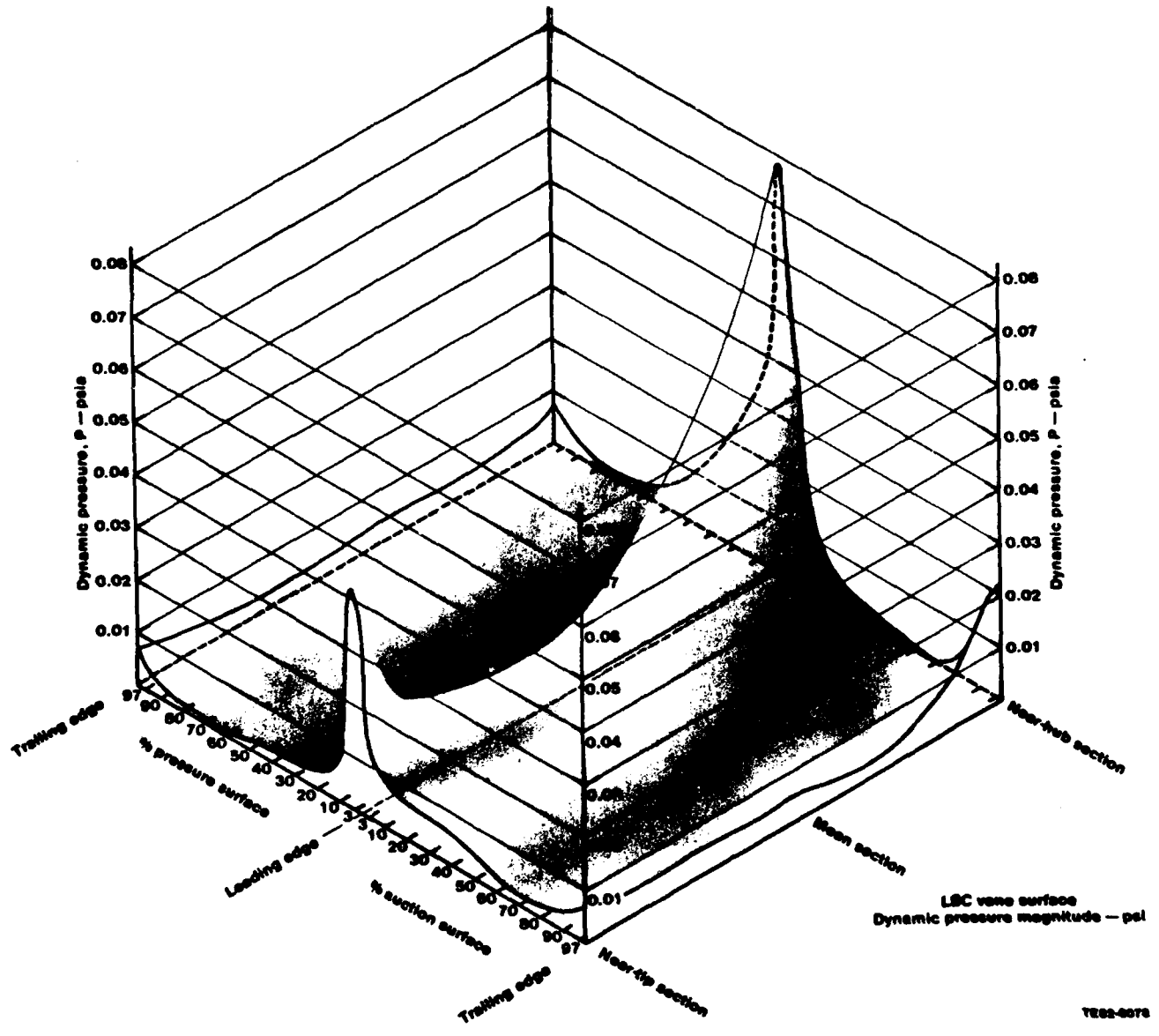

Figure 37. Unwrapped vane dynamic pressure distribution: 0.48% blade tip clearance, near-design operating conditions.

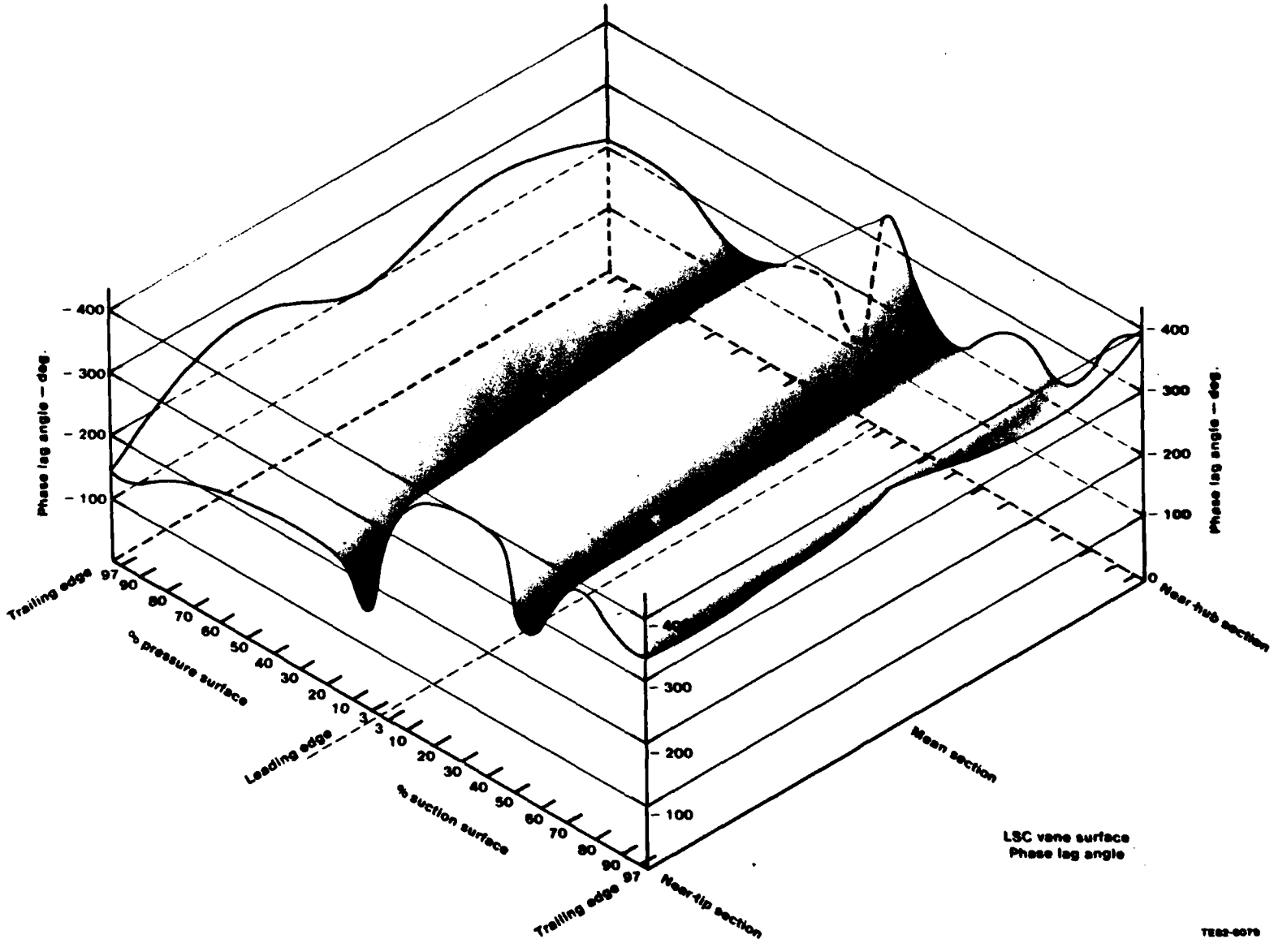

Figure 38. Unwrapped vane phase lag distribution: 0.48% blade tip clearance, near-design operating conditions.

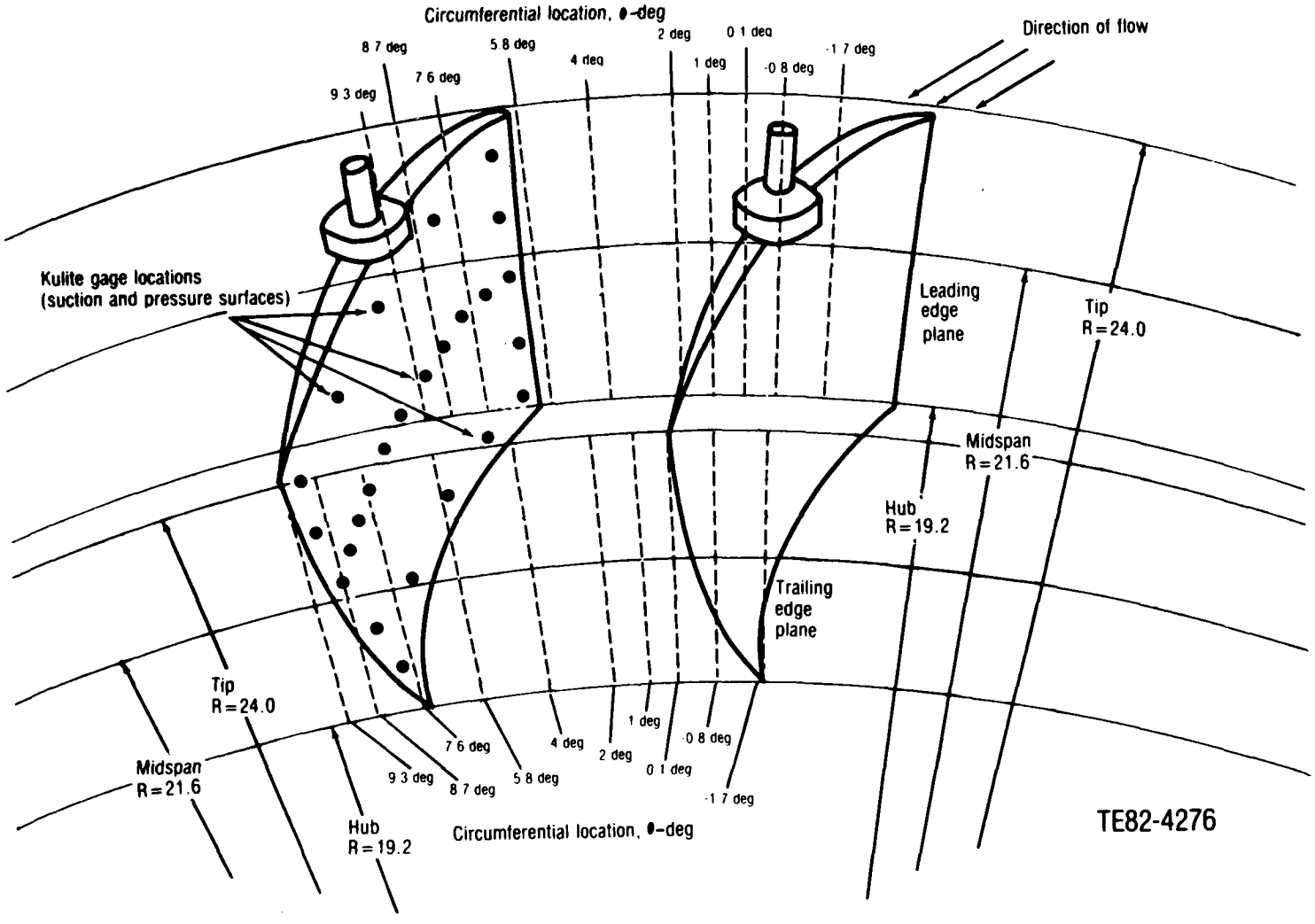

Figure 39. Vane Kulite gage and hot-wire anemometer probe locations.

For example, in the leading edge plane, the survey performed at θ = 5.8 deg was very near the leading edge of one of the vanes, and θ = 2 deg represents a near-midpassage circumferential location.

In the vane trailing edge plane, θ = 0.1 deg and 8.7 deg represents surveys performed near the trailing edge of the vanes. A circumferential location of θ = 4 deg represents a midpassage circumferential location in the vane trailing edge plane.

Figures 40, 41, and 42 illustrate, respectively, hot-wire signal results obtained from the vane inlet plane survey, the vane suction and pressure surface Kulite gage response, and the vane trailing edge hot-wire signals when the 0.48% span tip clearance configuration was operating at near-design speed, flow, and pressure ratio conditions.

Considering Figure 40 first, the two signals in each frame represent fluctuating velocity components in the transverse and streamwise directions. Near the midspan region (i.e., between r = 21.61 and r = 23.208), the blade wakes are seen to be well defined. However, as the hub is approached, the fluctuating signal increases in strength and the blade wake are less well defined. The condition is due to the boundary layer buildup with subsequent corner vortex formation on the blade hub endwall. Out near the tip, the blade trailing edge wake is still discernible, but the flow is dominated by the blade tip clearance vortex formation. A phase shift in the signals is apparent in the circumferential direction at constant radius; however, no significant phase variation is seen in the radial direction.

Figure 41 shows the axial and radial variation in suction and pressure Kulite gage response for the compressor operating at near-design conditions. It can be seen that the rotor wake-induced pressure signal is strong and well defined at blade passing frequency at the vane leading edge. Inside the passage, though, a high frequency disturbance is superimposed on the blade passing frequency signal and remains evident to the vane trailing edge. The condition is observed to occur at all of the instrumented radial sections.

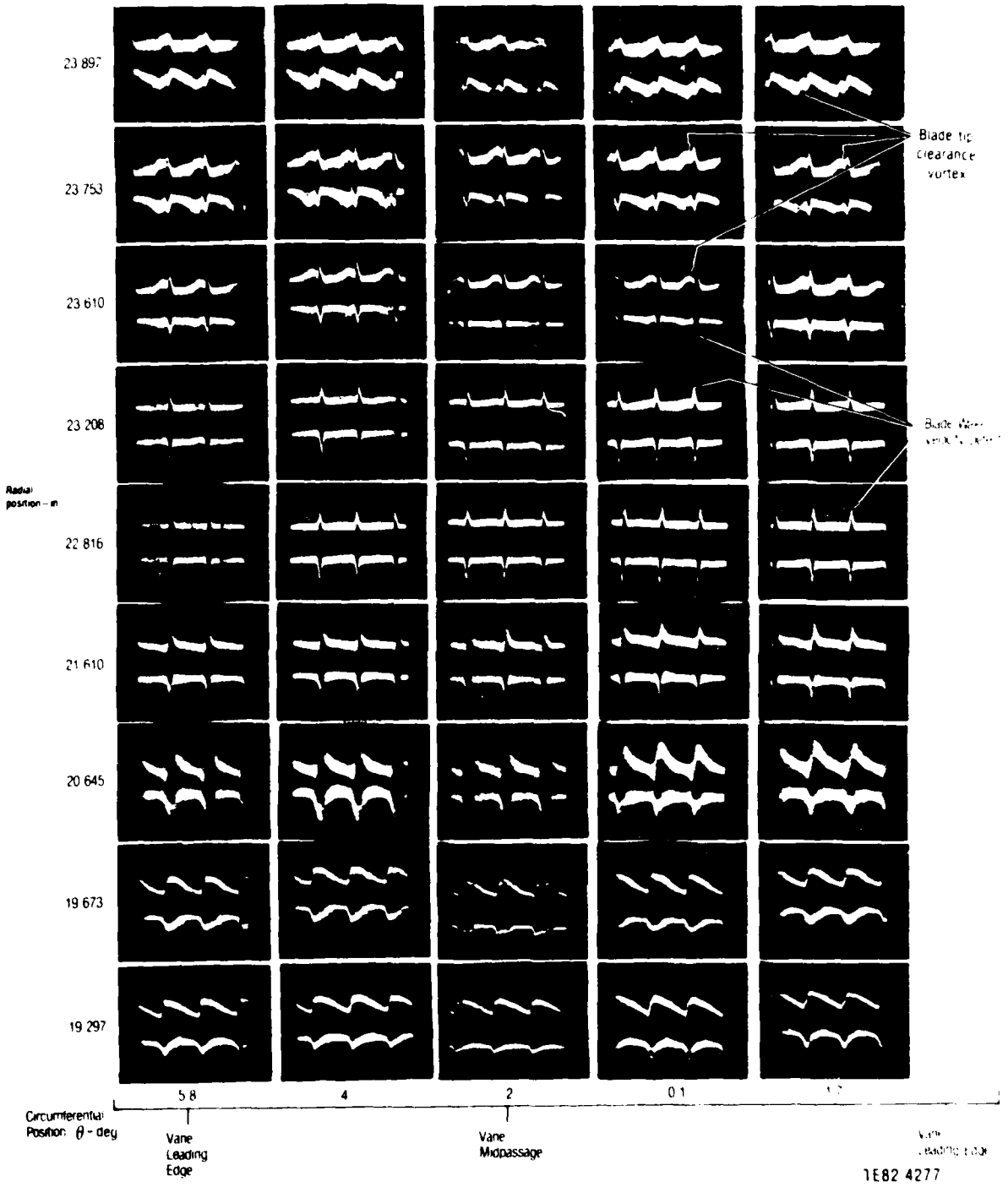

Figure 40. Design flow conditions--vane leading edge hot-wire radial and circumferential survey (0.48% span tip clearance).

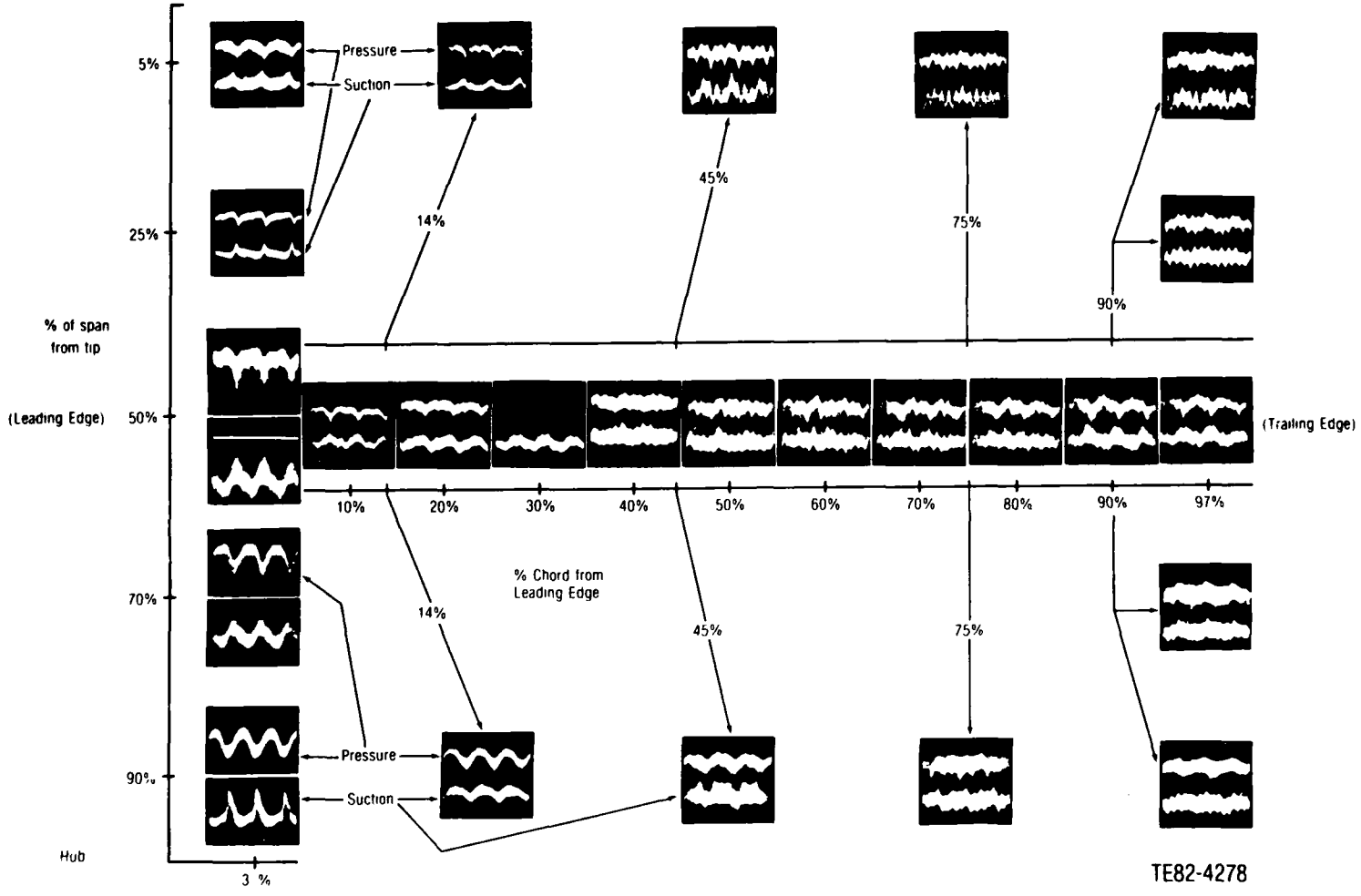

Figure 41. Design flow conditions--vane suction and pressure surface Kulite gage response (0.48% span tip clearance).

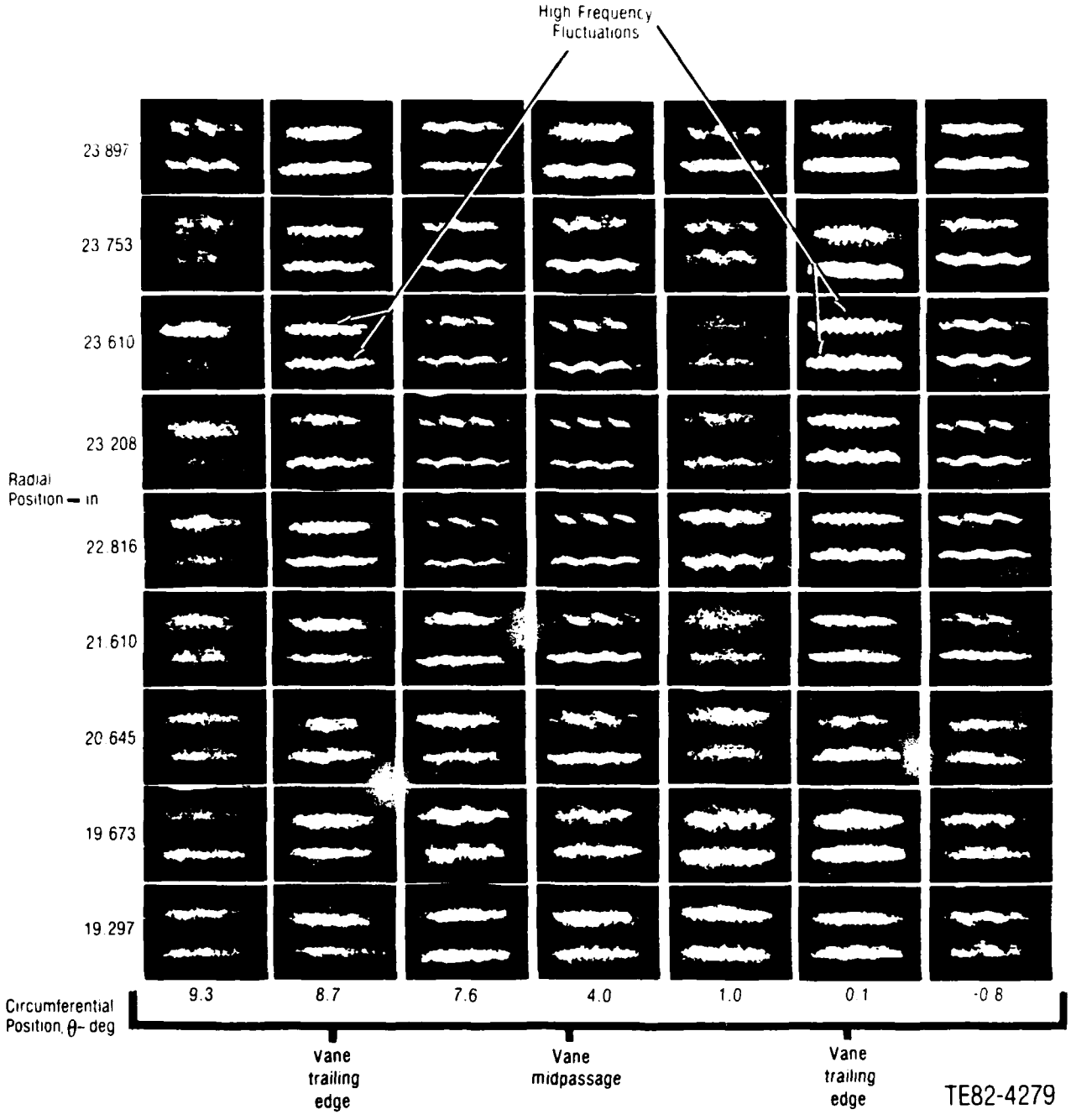

Figure 42. Design flow conditions--vane trailing edge hot-wire radial and circumferential survey (0.48% span tip clearance).

Considering now the vane trailing edge survey results of Figure 42, it can be seen that the signals are substantially attenuated from the leading edge plane levels. In the midpassage region (θ = 4 deg) the blade passage frequency disturbance is still apparent, but it becomes progressively less distinct as the endwall regions are approached. The circumferential locations of θ = 0.1 deg and 8.7 deg represent, at least in the outer half portion of the flow path, surveys performed along the trailing edges of adjacent vanes. The same higher frequency disturbance that was observed on the vane surface is noted at these two trailing edge locations.

This observation is documented first by considering Figure 43, which is a presentation of the harmonic content of each Kulite gage signal on the vane surface when the small tip clearance stage configuration was operating at near-design conditions. That figure shows the harmonic content of the first six harmonics of the gages placed at their respective chordwise locations on the vane at the hub, mean, and tip sections. The first harmonic is the blade passing frequency. Higher harmonics are disturbances that are superimposed on the blade passing frequency. Figure 43 shows that in the vane leading edge region, where the signal is somewhat sinusoidal and the blade passing frequency is well defined, the harmonic content of the signal is, principally, the first harmonic. As the flow proceeds along the vane surface, a fourth harmonic becomes apparent around 15%-20% chord on both surfaces and remains evident, particularly in the hub and tip regions all the way to the trailing edge.

Examination of the harmonic content of the vane leading edge hot-wire survey results of Figure 42 showed that nowhere was the fourth harmonic the dominate harmonic. However, it should be noted that, because of the fairly complicated blade wake signal, harmonic analysis of these signals did produce not only the dominate first harmonic but also higher harmonics that generally were of sizable magnitude. These higher harmonics progressively reduced in magnitude with ascending harmonic number.

In Figure 44, three outer radial locations at three circumferential positions (adjacent vane trailing edges and midpassage) were selected to demonstrate vane exit plane harmonic content. That illustration shows that it is principally the fourth harmonic that is dominant at the trailing edges, but it is not evi-

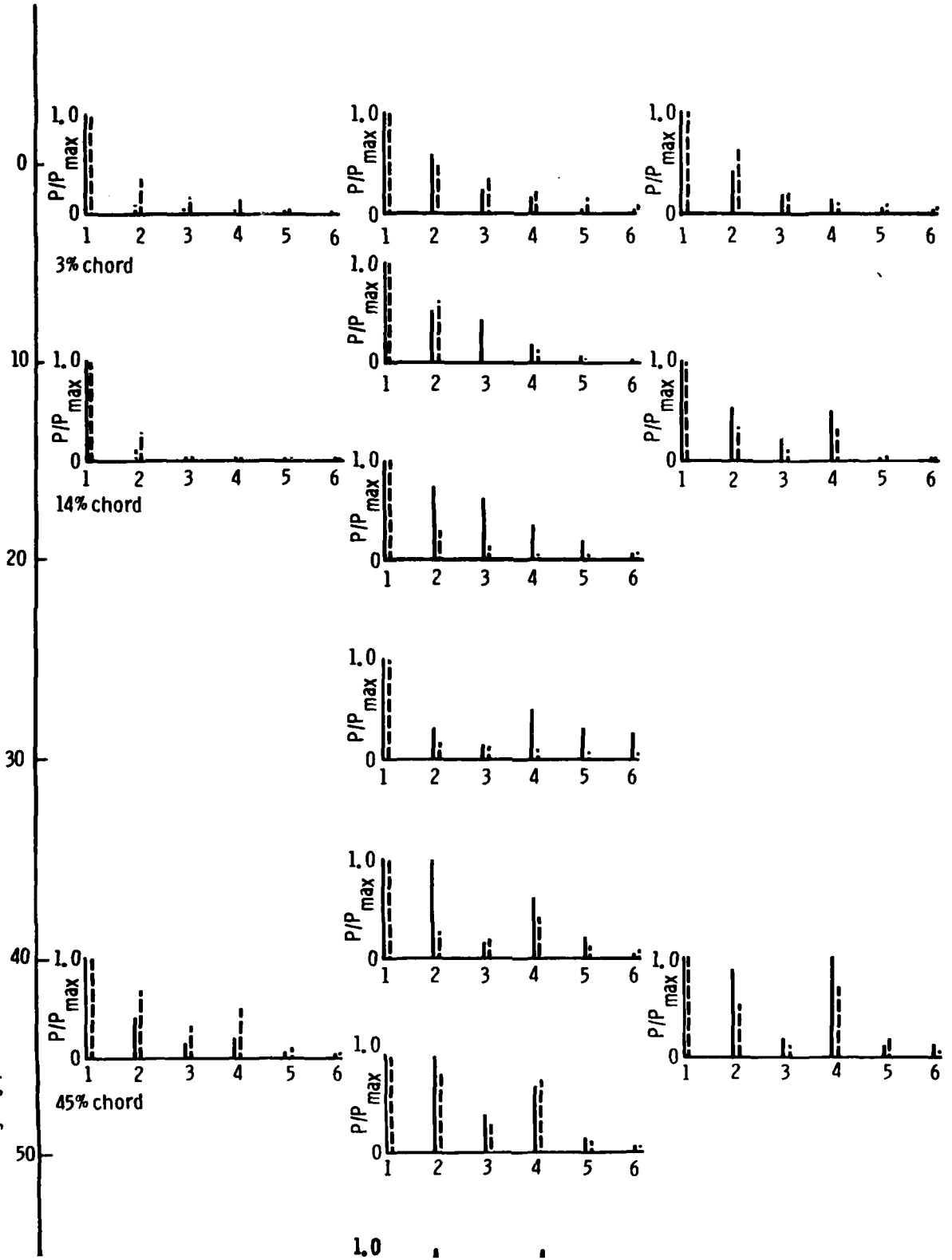
0
10
20
30
40
50
1.0
P/P max
0
1 2 3 4 5 6
3% chord
14% chord
45% chord
rd from leading edge, x/C—%

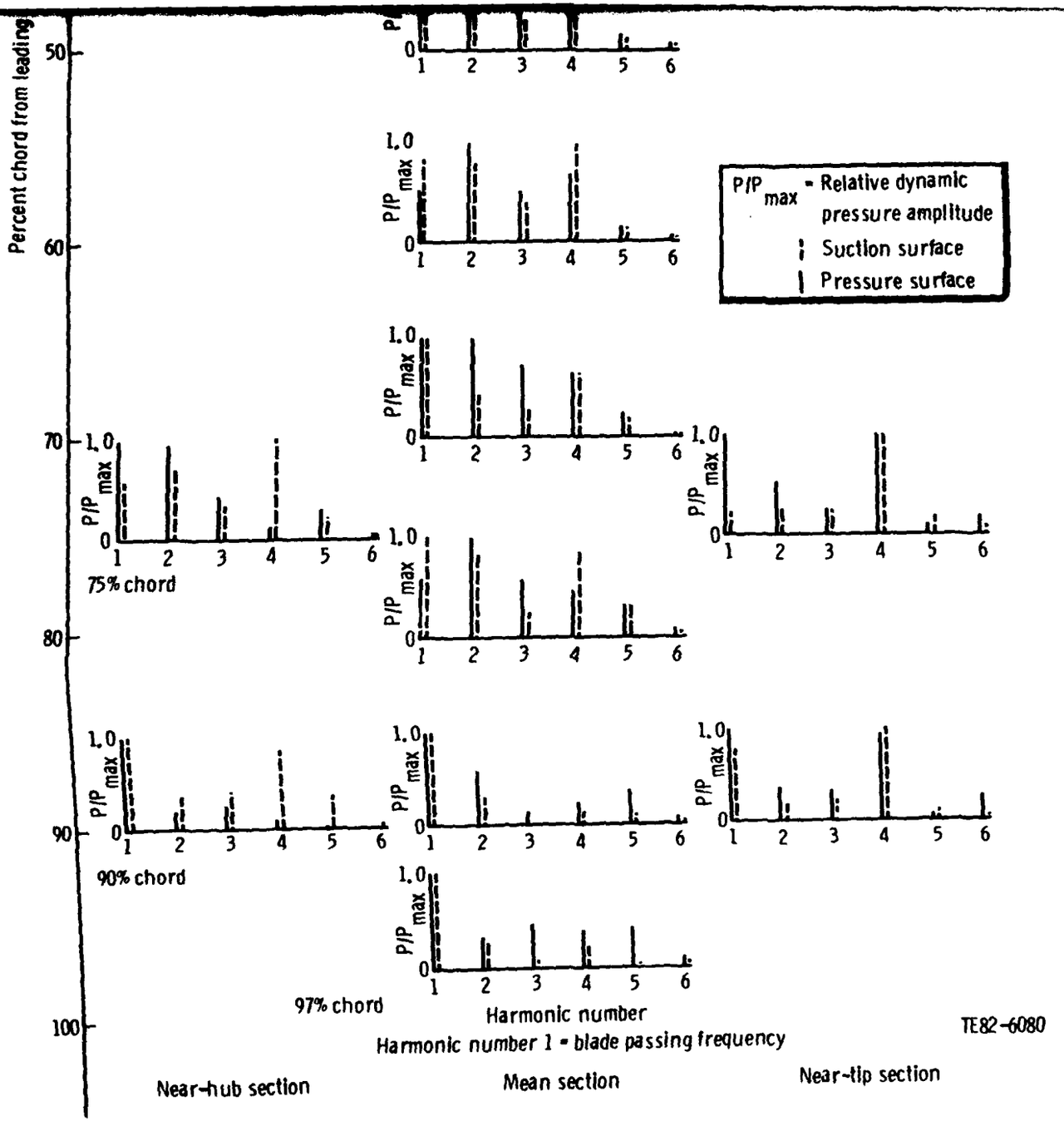

Figure 43. Vane surface distribution of dynamic pressure harmonic content for 0.48% blade tip clearance, near-design operating conditions, 100% speed.

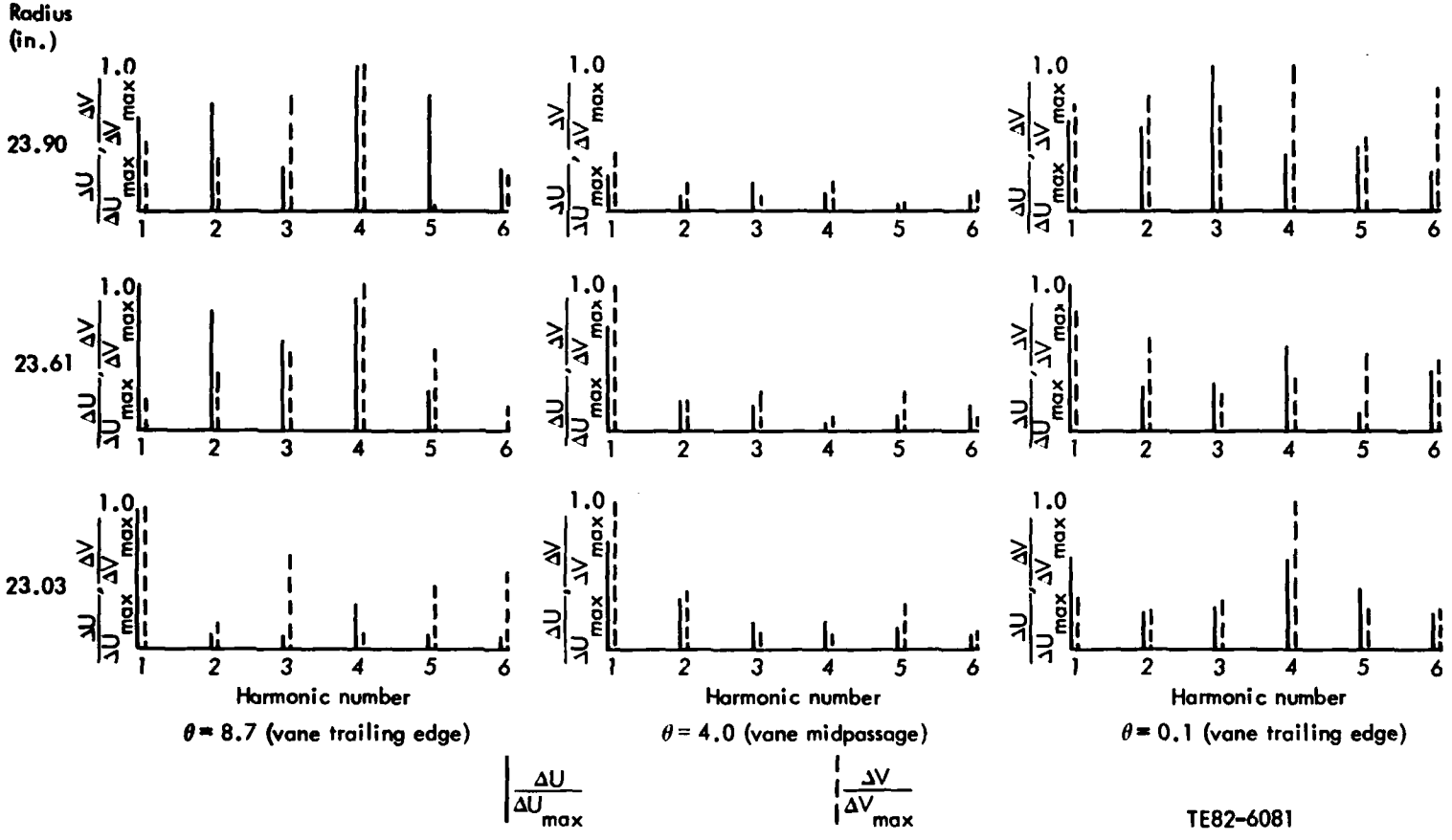

Figure 44. Vane trailing edge plane near-tip region fluctuating velocity harmonic content for 0.48% blade tip clearance, near-design operating conditions.

dent in the midpassage region. Thus, it is concluded that the high frequency disturbance is an airfoil surface condition and is, in fact, thought to be the result of Tollmien-Schlichting waves emanating from the transition region on the forward portion of the vane, along the vane surface to the trailing edge plane. This same phenomenon has been observed by Dring et al. (Ref. 3) on a dynamically instrumented, single-stage research turbine.

IV. CONCLUSIONS

Fluctuating static pressure and hot-wire wake measurements have been performed in the DDA single-stage low speed compressor operating over a range of flows, speeds, and pressure ratios with a small value (0.48% span) of blade tip clearance. Based on the analysis of these results and comparisons with similar but larger (3.0% span) tip clearance results, the following conclusions are drawn:

1. Rotor tip section trailing edge dynamic pressure results showed that suction and pressure surface measurements both approach the same magnitude of phase angle as the compressor stage was loaded from open throttle to design conditions.

2. Vane inlet radial/circumferential, hot-wire surveys showed poor flow conditions, which were generated within the rotor passage, produced large values of velocity level and overturning in the inner one-third of the annulus.

3. The quantity $\Delta V/U_{abs}$ has been identified as the disturbance quantity and is a measure of the magnitude of the blade wake velocity defect. In general, $\Delta V/U_{abs}$ increased with stage loading. Also, a reduction in blade tip clearance generally resulted in a reduction of $\Delta V/U_{abs}$ magnitude and phase lag angle in the vane leading edge tip region of the flow path.

4. The dynamic pressure across the airfoil section was substantially reduced when the blade tip clearance and, hence, wake forcing function were reduced. At the near-design operating condition, the vane tip leading edge dynamic pressure difference was reduced 32% when the blade tip clearance was reduced from 3.0% to 0.48% span.

5. The reduction in leading edge dynamic pressure was accomplished principally on the suction surface of the vane.

6. A substantial radial migration of the disturbance effects was noted for the large tip clearance configurations. Because of zero radial migration strip assumption of available gust analysis codes, for large tip clearance configurations those procedures should be limited to airfoil mean-section analysis.

7. In general, a reduction in blade tip clearance produced a reduction in vane tip region disturbance phase lag angle.

8. During the course of vane exit hot-wire surveys, a high frequency (fourth harmonic) was observed to occur along only the vane trailing edge span. This disturbance frequency correlated directly with a fourth harmonic disturbance that had been observed to develop on the vane surface around 15%-20% chord and to be present all the way to the trailing edge. A possible explanation for this high frequency disturbance is that it is the result of Tollmien-Schlichting waves emanating from the transition region on the forward portion of the vane.

V. RECOMMENDATIONS

The findings of this investigation included very limited dynamic pressure information for the compressor rotor system. It is recommended that a new program be initiated where the compressor rotor blades are heavily instrumented with very high quality surface dynamic pressure gages at several radial locations. The instrumented rotor, in conjunction with the in-place steady and dynamic instrumentation, would allow high quality investigations and determination of blade/vane interactions as functions of blade/vane axial gap, blade tip clearance, and stage operating condition. The research would certainly lead to improved understanding of aerodynamically induced vibration.

REFERENCES

1. R. L. Jay and J. L. Bettner, "Aerodynamically Induced Vibration," EDR 10840, September 1981.

2. B. Lakshminarayana, "Methods of Predicting the Tip Clearance Effects in Axial Flow Turbomachinery," Transactions of the ASME, Journal of Basic Engineering, Vol 92, 1970, pp 467-482.

3. S. M. Smith, "Discrete Frequency Sound Generation in Axial Flow Turbomachines," University of Cambridge, Department of Engineering Report CUED/A-Turbo 29, 1971.

4. J. A. Caruthers, "Aerodynamic Analysis of Cascade Airfoils in Unsteady Rotational Flow," Symposium on Aeroelasticity in Turbomachines, Lausanne, Switzerland, 8-12 September 1980.

5. "Research on Turbine Rotor-Stator Aerodynamic Interaction and Rotor Negative Incidence Stall," United Technologies Research Center, AFWAL-TR-81-2114, November 1981.

LIST OF SYMBOLS

AR	Aspect ratio, ℓ/C
C	True chord, in.
D	Diameter, in.
D_f	Diffusion factor
i	Incidence angle, $(\beta_1 - \beta_m)$, deg
l	Airfoil height, in.
le	Leading edge radius, in.
N	Shaft speed, rpm
$N/\sqrt{\theta}$	Corrected shaft speed, rpm
ΔP	Pressure difference across airfoil, $(P_{sp} - P_{ss})$, psia
R	Radial coordinate, in.
R_c	Pressure ratio
s	Airfoil spacing, in.
te	Trailing edge radius, in.
U_{abs}	Stator inlet midpassage freestream absolute velocity, ft/sec
U_t	Blade tip speed, ft/sec
$U_t/\sqrt{\theta}$	Blade corrected tip speed, ft/sec
ΔU	Streamwise fluctuating velocity component, ft/sec
ΔV	Transverse fluctuating velocity component, ft/sec
W	Flow rate, lb/sec
$W\sqrt{\theta}/\delta$	Corrected flow rate, lb/sec
x	Axial coordinate, in.
z	Coordinate from airfoil tip, in.

GREEK SYMBOLS

β_1	Inlet air angle, deg
β_2	Exit air angle, deg
δ	Ratio of compressor inlet total pressure to absolute pressure at standard sea level conditions
η	Efficiency, %
θ	Ratio of compressor inlet total temperature to total temperature at standard sea level conditions

θ	Circumferential coordinate, deg
σ	Solidity, σ = C/s
ϕ	Airfoil camber angle, deg
ϕ	Phase angle, deg
ω	Total pressure loss coefficient

SUBSCRIPTS

b	blade
h	hub
ΔP	dynamic pressure difference across vane
ps	pressure surface
ss	suction surface
t	tip
TT	Total-to-total
ΔU	Streamwise fluctuating component
ΔV	Transverse fluctuating component
v	vane